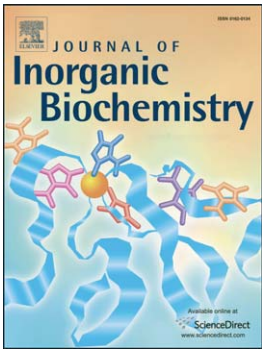

Tacrine-(hydroxybenzoyl-pyridone) hybrids as potential multifunctional anti-Alzheimer¡!–[INS]–¿'¡!–[/INS]–¿s agents: AChE inhibition, antioxidant activity and metal chelating capacity

Karam Chand, Hesham M. Alsoghier, Sílvia Chaves, M. Amélia Santos

PII: S0162-0134(16)30129-5
DOI: doi: 10.1016/j.jinorgbio.2016.05.005
Reference: JIB 9994

To appear in: *Journal of Inorganic Biochemistry*

Received date: 15 December 2015
Revised date: 2 May 2016
Accepted date: 10 May 2016

Please cite this article as: Karam Chand, Hesham M. Alsoghier, Sílvia Chaves, M. Amélia Santos, Tacrine-(hydroxybenzoyl-pyridone) hybrids as potential multifunctional anti-Alzheimer¡!–[INS]–¿'¡!–[/INS]–¿s agents: AChE inhibition, antioxidant activity and metal chelating capacity, *Journal of Inorganic Biochemistry* (2016), doi: 10.1016/j.jinorgbio.2016.05.005

Tacrine-(hydroxybenzoyl-pyridone) hybrids as potential multifunctional anti-Alzheimer´s agents: AChE inhibition, antioxidant activity and metal chelating capacity

Karam Chand[a)], Hesham M. Alsoghier[a,b)], Sílvia Chaves[a)*], M. Amélia Santos [a)*]

a) Centro de Química Estrutural, Instituto Superior Técnico, Universidade de Lisboa, Av. Rovisco Pais 1, 1049-001 Lisboa, Portugal.

b) South Valley University, Faculty of Science, Chemistry Department, 83523 Qena, Egypt.

Keywords: Hydroxybenzoyl-pyridones; Tacrine; Anti-neurodegeneratives; Anti-AChE activity; Anti-oxidant activity; Metal chelation.

* Corresponding authors:
(Sílvia Chaves) E-mail: silvia.chaves@tecnico.ulisboa.pt; Phone: +351-218419269
(M. Amélia Santos) E-mail: masantos@ist.utl.pt; Phone: +351-218419273

Abstract

Three novel potentially site-activated multitarget tacrine-(hydroxybenzoyl-pyridone) (TAC-HBP) hybrids were designed, synthesized and evaluated as acetylcholinesterase (AChE) inhibitors, antioxidants and biometal chelators. All of them are dual-binding site AChE inhibitors with activity in sub-micromolar range (IC_{50} = 0.57-0.78 μM), which is comparable to the parent tacrine, and have good 2,2-diphenyl-1-picrylhydrazyl (DPPH) radical scavenging capacity (EC_{50} = 204-249 μM) conferred by the hydroxybenzoyl-pyridone (HBP) moiety. Their chelating capacity towards redox-active and/or amyloid-β-binding metal ions (Fe(III), Cu(II)), Zn(II)) was evaluated by using 2′-hydroxy-4′-methoxybenzoyl-2-pyridone derivative as a model compound in 30% w/w DMSO/water medium. It was proved that the HBP moiety acts as a moderate/good chelator of these biometals (pFe = 13.9, pCu = 6.0 and pZn = 6.0 at pH 6.0, C_L/C_M = 10, $C_M = 10^{-6}$ M), being able to form complexes with β-phenol-keto coordination mode, and that this chelating ability is preserved in the TAC-HBP hybrids.

1. Introduction

Alzheimer's disease (AD) is a progressive neurological disease leading to memory impairment and loss of language, judgment and orientation, eventually causing incapacitation and death [1]. This is a multifaceted disease for which several factors, such as cholinergic dysfunction, deposits of amyloid-β (Aβ) and tau (τ)-protein as well as reduced blood supply in brain, are supposed to be relevant for its development [2]. The brains of AD patients display also other characteristic pathological features, such as metal ion (Fe, Cu, Zn) dyshomeostasis and elevated oxidative stress [3]. Metal ions, such as Cu and Zn, bind to Aβ peptides, thereby contributing to enable their aggregation, while deregulated redox active metal ions, Cu(I/II) and Fe(II/III), stimulate the overproduction of reactive oxygen species (ROS) with concomitant degradation of several cellular biomolecules (e.g. proteins, deoxyribonucleic acid (DNA), lipids).

The most frequently prescribed anti-AD drugs are cholinesterase inhibitors (ChEIs) that act by increasing acetylcholine (ACh) level in the brain via inhibition of acetylcholinesterase (AChE) and/or butyrylcholinesterase (BuChE) [4]. Tacrine (see Fig. 1), which was the first drug approved by the U.S. FDA for the palliative treatment of AD, showed reduction in the decline of cognitive performance due to inhibition of AChE [5], but it was discontinued because it turned out to be hepatotoxic. Regrettably, ChEIs have been proving to be inefficient in AD therapy being unable to delay or prevent the progression of this disease. In fact, due to the complex pathogenesis of AD and to the possible interconnection of several intervenient factors, an innovative therapeutic approach based on multi-target-directed ligands (MTDLs) has been applied in the search for potential ChEIs anti-AD drugs [6]. The most common strategy to design MTDLs is to connect two distinct classes of compounds in one molecule by choosing a proper spacer.

Since oxidative stress, as well as metal ion dyshomeostasis, are known to play important roles in the processes of AD pathogenesis, by preceding (biomolecule disruption) or provoking hallmark pathologies of this disease (neurofibrillary tangles, senile plaques, ROS) [7,8] it seems that compounds presenting both radical scavenging activity and capacity for biometal modulation in the brain may be useful for either the prevention or the therapy of AD.

Pyridin-2(1*H*)-ones (2-pyridones) have long been considered important building blocks in drug discovery due to the number of biologically active molecules containing this moiety. Along the last decades, several natural compounds with this core structure have emerged with numerous pharmacological activities, namely anti-AD (Huperzine A [9,10], AChEI and antioxidant) and antitumour (e.g. Camptothecin [11]), while many synthetic or semi-synthetic clinical drugs also enclose that non-toxic moiety [12] (see Fig. 1).

Therefore, as part of our interest on new polyfunctional drugs to combat AD, by conjugating an active AChEI moiety (e.g. tacrine) with a variety of functional groups [13-15], and also looking into the potential clinical application of tacrine and 2-pyridone moieties, we herein hypothesized the inclusion of a 2-hydroxybenzoyl-2-pyridone (HBP) derivative on such extra-functionalization. These tacrine-(hydroxybenzoyl-pyridone) (TAC-HBP) conjugates are expected to: a) exhibit AChE inhibition (tacrine moiety) and b) be able to tackle other pathways such as the oxidative stress found in the brain of AD patients, due to excess of redox-active (Cu, Fe) metal ions/free radicals, by chelators (HBP moiety) able to modulate misplaced redox-active metal ions and possessing anti-oxidant properties to scavenge free radicals. Under the followed design strategy, molecular modelling studies were performed of these TAC-HBP hybrids in which tacrine is linked through different alkyl spacers to the envisioned 2-pyridone moieties. These 2-pyridone moieties are based on a 5-(2-hydroxybenzoyl)-pyridin-2(1*H*)one scaffold with different ring substitutes (compounds **I**, see Fig. 1) and have already proved activity against c-Src kinase, over-expressed in various human cancers [16]. A synthetic approach for the preparation of tacrine conjugates **II** (see Fig. 1) with appropriate size linkers, previously established by docking studies, was implemented and afterwards compounds **II** were assayed in terms of AChE inhibition and anti-oxidant capacity - 2,2-diphenyl-1-picrylhydrazyl (DPPH) radical scavenging activity assays - while metal (Fe, Cu, Zn) chelating power was evaluated for a model compound (**I**, R=4'-OMe) and confirmed for a TAC-HBP hybrid (**II**, R=5´-OMe, n=1).

Fig. 1 - Molecular structure of: anti-AD drugs - tacrine and huperzine A –, antitumour camptothecin and HBP derivatives under study (**I**, **II**).

2. Experimental Section

2.1 Materials and methods

Analytical grade reagents were purchased from current suppliers and were used as delivered. Whenever necessary, solvents were dried according to standard methods [17]. The aqueous iron ($FeCl_3$, 0.0177 M), copper ($CuCl_2$, 0.015 M) and zinc ($ZnCl_2$, 0.0156 M) stock solutions were prepared from 1000 ppm standards (Titrisol) and their metal content was evaluated by atomic absorption. The iron stock solution was prepared in acid chloride excess, to prevent hydrolysis, and its exact concentration in HCl was accurately determined by the usual standard-addition method using 0.1 M HCl (Titrisol). This 0.1 M HCl solution, also used in calibration of the glass electrode, was prepared from a Titrisol ampoule. The titrant used in pH-potentiometric and spectrophotometric titrations was prepared from carbonate free commercial concentrate (Titrisol, KOH 0.1 M ampoules). The KOH solution was standardized by titration with a solution of potassium hydrogen phthalate and was discarded whenever the percentage of carbonate, determined by Gran's method [18], was greater than 0.5% of the total amount of base.

Reactions were monitored by precoated thin layer chromatography (TLC) plates (Merck silica gel $60F_{254}$); the spots were visualized either by UV light, or by spraying with 5% alcoholic $FeCl_3$ or ninhydrin solutions. Silica gel60 (0.061–0.2 mm) was used for column chromatography. Melting points were measured with a Leica Galen III hot stage apparatus and are uncorrected. The ^{1}H and ^{13}C NMR spectra were recorded on Bruker AVANCE III-400 (400 MHz, 100.5 MHz) and Bruker AVANCE III (300 MHz, 75.5 MHz) NMR spectrometers, at 25 °C using residual peaks of solvents as an internal standard. The chemical shift values are on a δ scale and the coupling constant values (*J*) are in Hertz. The following abbreviations are used: s = singlet, d = doublet, t = triplet, m = multiplet, dd = double doublet and brs = broad singlet. Peak attribution was, whenever necessary, confirmed by two-dimensional NMR experiments, namely correlation spectroscopy (COSY) and heteronuclear single quantum coherence spectroscopy (HSQC). The antioxidant and AChE inhibitory activities were determined by using a Perkin Elmer Lambda 35 spectrophotometer equipped with a temperature programmer PTP 1+1 Peltier System, using thermostated (T = 25.0±0.1 °C) 1 cm path length cells. Electrospray ionization-mass spectrometry (ESI-MS) experiments were carried out on a LCQ Fleet mass spectrometer operated in the ESI positive and negative ion modes (Thermo Scientific).

2.2 Molecular modeling studies of TAC-HBP hybrids

The docking calculations were performed following a procedure identical to that previously reported [19]. The X-ray crystallographic structure of acetylcholinesterase *Torpedo californica* AChE (*Tc*AChE) complexed with an inhibitor was taken from RCSB Protein Data Bank (PDB entry 1ODC), in order to be used as receptor in the docking simulations. The original complex structure was treated using Maestro v. 9.3 [20], by removing the original ligand, solvent and co-crystalization molecules and adding hydrogen atoms. This program was also used to design the ligand structures, which were submitted to random conformational search (RCS) of 1000 cycles and 2500 optimization steps with the program Ghemical v 2.0 [21]. The ligands were docked into the AChE structure, using GOLD v. 5.1. [22] with the default parameters of GOLD (except 'allow early termination' option) and the Astex Statistical Potential (ASP) scoring function. The zone of interest was defined as the residues within 10 Å from the original position of the ligand in the crystal structure.

2.3 Synthesis of the compounds

2.3.1. General procedure for the synthesis of *N*-substituted HBP derivatives (6-11):

To a solution of (4-oxo-4*H*-chromen-3-yl)acrylate (**3-5**) (4 mmol) and aminoalkane or *t*-butylaminoethylcarbamate (4.1 mmol) in ethanol (50 mL) was added triethylamine (2 drops), and the reaction mixture was refluxed for 8-10 h. The progress of reaction was monitored on TLC. On completion of reaction, the mixture was cooled to room temperature, and the solvent was evaporated under reduced pressure. The crude product was either purified by column chromatography over silica gel (100–200 mesh) in 2-3% dichloromethane/methanol or through crystallisation in CH_3OH-CH_3CN system, to give HBP derivatives (**6**-**11**) in 74-85% yield. Although spectral data for compounds **6**-**8** has been recently reported [16,23], their full characterization is herein presented, along with that for compounds **9**-**11**, since the antioxidant activity of compounds **6**-**8** is evaluated on this article. See also Supplementary Information with ^{1}H and ^{13}C NMR spectra for compounds **6**-**17**.

5-(2-Hydroxy-4-methoxybenzoyl)-1-isopropylpyridin-2(1*H*)-one (**6**): The title compound **6** was obtained as a light yellow coloured solid with 85 % yield by following the literature reported reaction of (*E*)-ethyl 3-(7-methoxy-4-oxo-4*H*-chromen-3-

yl)acrylate (2 mmol) with isopropyl amine (2.2 mmol) [23]; mp = 139-141 ^{o}C; ^{1}H NMR (400 MHz, $CDCl_3$): δ = 1.42 (d, 6H, *J* = 4.0 Hz, C*H*$(CH_3)_2$), 3.87 (s, 3H, OCH_3), 5.26-5.32 (m, 1H, $(CH_3)_2CH$), 6.47 (d, 1H, *J* = 8.0 Hz, H-5'), 6.52 (s, 1H, H-3'), 6.64 (d, 1H, *J* = 8.0 Hz, H-6'), 7.47 (d, 1H, *J* = 8.0 Hz, H-3), 7.70 (dd, 1H, *J* = 4.0 & 8.0 Hz, H-4), 7.94 (s, 1H, H-6), 12.24 (brs, 1H, OH); ^{13}C NMR (100.5 MHz, $CDCl_3$): δ = 21.97, 47.52, 55.69, 101.50, 107.59, 112.58, 118.04, 119.47, 133.28, 138.40, 161.78, 165.83, 166.18, 194.01; ESI-MS (m/z): Calculated for $C_{16}H_{17}NO_4$ 287.1158, found $[M+H]^+$ 288.43 and $[2M]^+$ 574.98; Analysis calc. for $C_{16}H_{17}NO_4$.0.030 CH_3CN: C 66.89, H 5.96, N 4.88, %; found: C 67.16, H 6.04, N 4.91 %.

5-(2,4-dihydroxybenzoyl)-1-isopropylpyridin-2(1*H*)-one (**7**): The title compound **7** was obtained as a light yellow coloured solid with 78% yield by following the literature reported reaction of (*E*)-ethyl 3-(7-hydroxy-4-oxo-4*H*-chromen-3-yl)acrylate (2 mmol) with isopropyl amine (2.1 mmol) [23]; m.p. = 198-200 ^{o}C; ^{1}H NMR (400 MHz, DMSO-d_6): δ = 1.32 (d, 6H, *J* = 8.0 Hz, C*H*$(CH_3)_2$), 4.99-5.06 (m, 1H, $(CH_3)_2CH$), 6.37-6.40 (m, 2H, H-5' & H-3'), 6.46 (d, 1H, *J* = 8.0 Hz, H-3), 7.40 (d, 1H, *J* = 8.0 Hz, H-6'), 7.69 (d, 1H, *J* = 8.0 Hz, H-4), 8.11 (d, 1H, *J* = 4.0 Hz, H-6), 10.48 (brs, 1H, OH), 11.44 (brs, 1H, OH); ^{13}C NMR (100.5 MHz, DMSO-d_6): δ = 21.54, 47.80, 103.22, 108.44, 114.21, 117.56, 118.89, 134.19, 138.86, 140.54, 161.37, 162.48, 164.19, 192.83; Calculated for $C_{15}H_{15}NO_4$ 273.1001, found $[M+H]^+$ 274.27 and $[M-H]^+$ 272.87. Analysis calc. for $C_{15}H_{15}NO_4$.0.020 CH_3CN: C 65.91, H 5.53, N 5.13 %; found: C 65.99, H 5.58, N 5.12%.

5-(2,5-Dihydroxybenzoyl)-1-isopropylpyridin-2(1*H*)-one (**8**): The title compound **8** was obtained as a light yellow coloured solid with 68% yield by following the literature reported reaction of (*E*)-ethyl 3-(6-hydroxy-4-oxo-4*H*-chromen-3-yl)acrylate (2 mmol) with isopropyl amine (2.1 mmol) [16]; mp = 156-158 ^{o}C; ^{1}H NMR (400 MHz, MeOD-d_4): δ = 1.40 (d, 6H, J = 4.0 Hz, C*H*$(CH_3)_2$), 5.13-5.20 (m, 1H, $(CH_3)_2CH$), 6.57 (d, 1H, *J* = 8.0 Hz, H-3), 6.83 (s, 1H, H-6'), 6.86 (d, 1H, *J* = 8.0 Hz, H-3'), 6.95 (dd, 1H, , *J* = 4.0 & 8.0 Hz, H-4'), 7.89 (dd, 1H, *J* = 4.0 & 8.0 Hz, H-4), 8.18 (d, 1H, *J* = 4.0 Hz, H-6); ^{13}C NMR (100.5 MHz, $CDCl_3$): δ = 21.84, 48.76, 115.94, 118.10, 118.21, 119.36, 119.74, 125.54, 138.69, 139.77, 149.17, 156.14, 162.23, 194.79; Calculated for $C_{15}H_{15}NO_4$ 273.1001, found $[M+H]^+$ 274.26 and $[2M]^+$ 546.71; Analysis calc. for $C_{15}H_{15}NO_4$.0.010 CH_3CN: C 65.91, H 5.53, N 5.13 %; found: C 65.80, H 5.51, N 5.09%.

t-Butyl 2-(5-(2-hydroxy-4-methoxybenzoyl)-2-oxopyridin-1(2*H*)-yl)ethylcarbamate (**9)**: The title compound (**9**) was obtained from the reaction of (*E*)-ethyl-3-(7-methoxy-4-oxo-4*H*-chromen-3-yl)acrylate (**4**) with *t*-butyl 2-aminoethylcarbamate as a light yellow solid in 83% yield by following the general procedure. mp: 167-168 ^{o}C. ^{1}H NMR (400 MHz, DMSO-d_6): δ 1.24 (s, 9H, -OC(CH_3)$_3$), 3.24 (brs, 2H, H-2''), 3.81 (s, 3H, OCH$_3$), 3.97 (brs, 2H, H-1''), 6.46 (d, 1H, *J* = 8.0 Hz, H-5'), 6.52-6.54 (m, 2H, H-3' & H-6′), 6.92 (t, 1H, *J* = 8.0 Hz, CON*H*), 7.54 (d, 1H, *J* = 8.0 Hz, H-3), 7.73-7.76 (m, 1H, H-4), 8.01 (s, 1H, H-6), 11.36 (brs, 1H, OH); ^{13}C NMR (100.5 MHz, DMSO-d_6): δ 28.45, 38.70, 50.05, 56.03, 78.36, 101.84, 107.01, 115.44, 116.63, 119.17, 133.62, 139.43, 145.94, 156.13, 161.87, 162.02, 164.87, 192.65; ESI-MS (m/z): Calculated for $C_{20}H_{24}N_2O_6$ 388.16, found $[M]^+$ 388.94 and $[M-H]^+$ 387.31.

t-Butyl 2-(5-(2-hydroxy-5-methoxybenzoyl)-2-oxopyridin-1(2*H*)-yl)ethylcarbamate (**10**): The title compound (**10**) was obtained from the reaction of (*E*)-ethyl-3-(6-methoxy-4-oxo-4*H*-chromen-3-yl)acrylate (**5**) with *t*-butyl 2-aminoethylcarbamate as a light yellow solid in 81% yield by following the general procedure. mp: 145-146 ^{o}C. ^{1}H NMR (400 MHz, DMSO-d_6): δ 1.25 (s, 9H, -OC(CH_3)$_3$), 3.21-3.23 (m, 2H, H-2''), 3.71 (s, 3H, OCH$_3$), 3.93-3.94 (m, 2H, H-1''), 6.43-6.46 (d, 1H, H-3), 6.82 (s, H-6'), 6.88-6.90 (m, 2H, CON*H* & H-3') 7.00 (d, 1H, *J* = 8.0 Hz, H-4'), 7.73-7.76 (m, 1H, H-4), 8.00 (s, 1H, H-6), 9.66 (brs, 1H, OH); ^{13}C NMR (100.5 MHz, DMSO-d_6**)**: δ 28.46, 50.19, 55.96, 56.49, 78.33, 113.97, 116.91, 118.18, 118.98, 119.40, 125.54, 139.12, 146.66, 149.91, 152.42, 156.09, 161.98, 191.70. ESI-MS (m/z): Calculated for $C_{20}H_{24}N_2O_6$ 388.16, found $[M+Na]^+$ 411.15 and $[M-H]^+$ 387.05.

t-Butyl (4-(5-(2,4-dihydroxybenzoyl)-2-oxopyridin-1(2H)-yl)butyl)carbamate (**11**): The title compound (**11**) obtained from the reaction of (*E*)-ethyl 3-(7-hydroxy-4-oxo-4H-chromen-3-yl)acrylate (**3**) with *t*-butyl 2-aminoethylcarbamate as a light yellow solid in 81% yield by following the general procedure. mp: 190-192 ^{o}C; ^{1}H NMR (400 MHz, DMSO-d_6): δ 1.34-1.38 (m, 11H, -OC(CH_3)$_3$ & H-3''), 1.59-1.62 (m, 2H, H-2''), 2.91-2.93 (m, 2H, H-4''), 3.95 (t, 2H, *J* = 8.9 Hz, H-1''), 6.35 (s, 1H, H-3'), 6.38 (d, 1H, *J* = 8.0 H-5'), 6.45 (d, 1H, *J* = 8.0 Hz, H-3), 6.81 (t, 1H, *J* = 8.0 Hz, CO*NH*), 7.40-7.43 (m, 1H, H-6'), 7.71 (d, 1H, *J* = 8.0 Hz, H-4), 8.22 (s, 1H, H-6), 10.47 (brs, 1H, OH), 11.41 (brs, 1H, OH); ^{13}C NMR (100 MHz, DMSO-d_6): δ 19.00, 26.53, 27.03, 28.69, 49.33, 56.49, 77.91, 103.22, 108.39, 114.15, 117.27, 119.03, 134.25, 139.59, 144.86, 156.10,

161.73, 162.54, 164.17, 192.89. ESI-MS (m/z): Calculated for $C_{21}H_{26}N_2O_6$ 402.18, found $[M+Na]^+$ 425.10 and $[M-H]^+$ 401.10

2.3.2. General procedure for the synthesis of free amino alkyl *N*-substituted HBP derivatives (12-14):

To the ice cold solution of the *Boc* protected HBP derivatives (**9-11**) (0.5 mmol) in 20 mL dichloromethyl (DCM) was added trifluoroacetic acid (TFA, 0.5 mL) dropwise, and the reaction mixture was stirred at 0-5 ^oC for 30 min. Then reaction temperature was allowed to attain room temperature and stirred at room temperature (RT) for 7-8 hrs. The progress of reaction was monitored on TLC. On completion, reaction mixture was neutralized with 15 mL of 30% ammonia solution. The reaction mixture was then subjected to extraction by adding 2 g of NaCl (to make the aqueous layer saturated) and additional 3×15 mL of DCM. The evaporation of combined organic layer under reduced pressure after drying over anhydrous Na_2SO_4, resulted into free amino alkyl substituted HBP derivatives (**12-14**) in 88-92% yield.

1-(2-aminoethyl)-5-(2-hydroxy-4-methoxybenzoyl)pyridin-2(1*H*)-one (**12**): The title compound (**12**) was obtained from the hydrolysis of *Boc* group of compound **9** with TFA as a greenish yellow solid in 92% yield by following the general procedure. mp: 150-152^oC. ^1H NMR (400 MHz, DMSO-d_6): δ 2.41-243 (m, 2H, H-2''), 3.83 (s, 3H, OCH3), 4.05 (brs, 2H, H-1''), 6.46-649 (m, 1H, H-5'), 6.55-6.57 (m, 2H, H-3' & H-6′), 7.54 (d, 1H, *J* = 8.0 Hz, H-3), 7.74 (d, 1H, *J* = 8.0 Hz, H-4), 8.19 (s, 1H, H-6), 11.43 (brs, 1H, OH); ^{13}C NMR (100.5 MHz, DMSO-d_6): 46.82, 56.04, 57.62, 101.71, 107.02, 116.52, 118.91, 133.61, 139.59, 145.98, 161.92, 164.99, 192.94; ESI-MS (*m/z*): $C_{15}H_{16}N_2O_4$ 288.11, found $[M + H]^+$ 289.23.

1-(2-Aminoethyl)-5-(2-hydroxy-5-methoxybenzoyl)pyridin-2(1*H*)-one (**13**): The title compound (**13**) was obtained from the hydrolysis of *Boc* group of compound **10** with TFA as a greenish yellow solid in 88% yield by following the general procedure. mp: 159-161 ^oC. ^1H NMR (400 MHz, DMSO-d_6): δ 2.43 (t, 2H, *J* = 8.0 Hz, H-2''), 3.65 (s, 3H, OCH_3), 3.98 (t, 2H, *J* = 8.0 Hz, H-1''), 6.37-6.40 (m, 1H, H-3), 6.80 (d, 1H, *J* = 4.0 Hz, H-3'), 6.83-6.85 (m, 1H, H-6'), 6.95 (dd, 1H, *J* = 4.0 & 8.0 Hz, H-4'), 7.69 (dd, 1H, *J* = 4.0 & 8.0 Hz, H-4), 8.13 (d, 1H, *J* = 4.0 Hz, H-6), 9.82 (brs, 1H, OH); ^{13}C NMR (100.5 MHz, DMSO-d_6): δ 46.80, 55.99, 57.71, 114.33, 116.70, 118.01, 118.72, 119.21,

125.45, 139.07, 146.94, 150.10, 152.32, 161.83, 191.94; ESI-MS (*m/z*): Calculated for $C_{15}H_{16}N_2O_4$ 288.11, found $[M+H]^+$ 289.15.

1-(4-Aminobutyl)-5-(2,4-dihydroxybenzoyl)pyridin-2(1*H*)-one (**14**): The title compound (**14**) was obtained from the hydrolysis of the *Boc* group of compound **11** with TFA as a light yellow solid in 88% yield by following the general procedure. mp 185-187 ^oC. ^1H NMR (400 MHz, DMSO-d_6): δ 1.43-1.47 (m, 2H, H-3"), 1.67-1.71 (m, 2H, H-2"), 2.69 (t, 2H, *J* = 8.0 Hz, H-4"), 3.98 (t, 2H, *J* = 8.0 Hz, H-1"), 6.11 (s, 1H, H-3'), 6.19 (d, 1H, *J* = 8.0 Hz, H-3), 6.44-6.47 (m, 1H, H-5'), 7.30-733 (m, 1H, H-6'), 7.69-7.72 (m, 1H, H-4), 8.16 (s, 1H, H-6), 10.42 (brs, 1H, OH), 11.42 (brs, 1H, OH); ^{13}C NMR (100 MHz, DMSO-d_6): δ 26.25, 26.70, 49.02, 56.49, 103.66, 110.81, 111.16, 117.70, 118.98, 134.11, 139.81, 143.87, 161.74, 164.56, 170.44, 191.49. ESI-MS (*m/z*): Calculated for $C_{16}H_{18}N_2O_4$ = 303.13, found $[M+H]^+$ 303.24.

2.3.3. General procedure for the synthesis of TAC-HBP hybrids (15-17):

Firstly, the mixture of 9-chloro-1,2,3,4-tetrahydroacridine (**2**, 0.4 mmol) and phenol (0.2 mmol) was heated with potassium iodide at 50 ^oC for 10 min. When reaction mixture became a dense oily material, free aminoalkyl substituted HBP derivatives (**12-14**, 0.4 mmol) were added to it and reaction mixture was heated at 165-170 ^oC for next 15 min. Accomplishment of reaction was monitored on TLC. On completion, the crude reaction mixture was cooled to RT and purified by column chromatography over silica gel 60 (0.061–0.2 mm) in 4-5% methanol/dichloromethane to give TAC-HBP hybrids (**15-17**) in 28-45% yield.

5-(2-hydroxy-4-methoxybenzoyl)-1-(2-((1,2,3,4-tetrahydroacridin-9-yl)amino)ethyl)pyridine-2(1*H*)-one (**15**): Title compound (**15**) was obtained by reaction of **2** with amine (**12**) as a light yellow solid in 28% yield by following the general procedure. mp: 259-260 ^oC; ^1H NMR (300 MHz, DMSO-d_6): δ 1.80 (brs, 4H, H-2‴ & H-3‴), 2.59 (brs, 2H, H-1‴), 2.96 (brs, 2H, H-4‴), 3.82 (s, 3H, OCH_3), 4.25-4.26 (m, 2H, H-1″), 4.35-4.36 (m, 2H, H-2″), 6.43-6.46 (m, 2H, H-3′ and H-3), 6.52 (d, 1H, *J* = 3.0 Hz, H-5′), 7.39 (m, 1H, H-4), 7.54 (t, 1H, *J* = 8.0 Hz, H-7‴), 7.68 (m, 1H, *J* = 3.0 & 9.0 Hz, H-6′), 7.77-7.79 (m, 2H, *NH* & H-5‴), 7.85 (t, 1H, *J* = 6.0, H-6‴) 8.09 (brs, H-6), 8.35 (d, 1H, *J* = 9.0 Hz, H-8‴), 11.21 (brs, 1H, OH); ^{13}C NMR (75.4 MHz, DMSO-d_6): δ 20.72, 21.83, 24.50, 28.51, 46.73, 50.24, 56.06, 101.82, 106.91, 112.38, 115.59,

116.16, 117.53, 118.95, 119.78, 125.23, 125.75, 133.41, 138.16, 140.08, 145.39, 151.63, 156.43, 161.63, 162.43, 164.82, 192.25; ESI-MS (*m/z*): Calculated for $C_{28}H_{27}N_3O_4$ $[M+H]^+$ 470.21, found 470.38. Analysis calc. For ($C_{28}H_{27}N_3O_4$. 0.025 H_2O): C 71.62, H 5.80, N 8.95 %; found: C 71.77, H 5.87, N 8.98%.

5-(2-hydroxy-5-methoxybenzoyl)-1-(2-((1,2,3,4-tetrahydroacridin-9-yl)amino)ethyl)pyridin-2(1*H*)-one (**16**): Title compound (**16**) was obtained by reaction of **2** with amine (**13**) as a light yellow solid in 45% yield by following the general procedure. mp: 143-145 ^oC; ^1H NMR (400 MHz, DMSO-d_6): δ 1.78 (brs, 4H, H-2‴ & H-3‴), 2.57 (brs, 2H, H-1‴), 2.94 (brs, 2H, H-4‴), 3.67 (s, 3H, OCH_3), 4.07-4.08 (m, 2H, H-1″), 4.30-4.32 (m, 2H, H-2″), 6.41-6.44 (m, 1H, H-3), 6.77 (d, 1H, *J* = 4.0 Hz, H-3′), 6.91(d, 1H, *J* = 8.0 Hz, H-4′), 6.99-7.00 (dd, 1H, *J* = 4.0 & 8.0 Hz, H-4), 7.27 (brs, 1H, N*H*), 7.44 (t, 1H, *J* = 8.0 Hz, H-7‴), 7.70 (dd, 1H, *J* = 4.0 & 8.0 Hz, H-4′), 7.74 (t, 1H, *J* = 8.0 Hz, H-6‴), 7.83-785 (m, 2H, H-6′ & H-5‴), 8.15 (d, *J* = 4.0 Hz, H-6), 8.24 (d, 1H, *J* = 8.0 Hz, H-8‴), 9.73 (brs, 1H, OH); ^{13}C NMR (100 MHz, DMSO-d_6): δ 21.22, 22.13, 24.65, 29.84, 46.81, 50.38, 55.35, 113.56, 114.01, 117.25, 117.50, 118.21, 118.77, 119.45, 122.08, 123.97, 124.69, 125.18, 125.37, 131.83, 139.76, 146.28, 149.96, 152.36, 153.33, 154.67, 162.48, 191.60; ESI-MS (*m/z*): Calculated for $C_{28}H_{27}N_3O_4$ 469.20, found $[M+H]^+$ 470.39. Analysis calc. for ($C_{28}H_{27}N_3O_4$. 0.005 H_2O): C 71.62, H 5.80, N 8.95 %; found: C 71.66, H 5.93, N 9.03%.

5-(2,4-Dihydroxy-benzoyl)-1-[4-(1,2,3,4-tetrahydro-acridin-9-ylamino)-butyl]-1*H*-pyridin-2-one (**17**): Title compound (**17**) was obtained by reaction of **2** with amine (**14**) as a light yellow solid in 33% yield by following the general procedure. mp: 264-266 ^oC; ^1H NMR (400 MHz, DMSO-d_6): δ 1.73 (brs, 4H, H-2" & H-3"), 1.83 (brs, 4H, H-2‴ & H-3‴), 2.63 (brs, 2H, H-1‴), 2.97 (brs, 2H, H-4‴), 3.88-3.89 (m, 2H, H-4″), 4.0 (brs, 2H, H-1″), 6.34-6.35 (m, 2H, H-3' and H-3), 6.42 (d, 1H, *J* = 8.0 Hz, H-5′), 7.36-7.39 (m, 1H, H-4), 7.56 (t, 1H, *J* = 8.0 Hz, H-7‴), 7.68 (d, 1H, *J* = 8.0 Hz, H-6′), 7.72 (brs, 1H, *NH*), 7.77-7.80 (m, 1H, H-5‴), 7.86 (t, 1H, *J* = 8.0, H-6‴) 8.19 (d, 1H, *J* = 4.0 Hz, H-6), 8.36 (d, 1H, *J* = 8.0 Hz, H-8‴), 10.52 (brs, 1H, OH), 11.41 (brs, 1H, OH); ^{13}C NMR (100 MHz, DMSO-d_6): δ 20.72, 21.82, 24.30, 26.14, 27.06, 28.42, 47.15, 49.18, 103.23, 108.37, 111.88, 114.08, 115.95, 117.29, 118.96, 119.56, 125.59, 133.23, 134.20, 138.25, 139.64, 144.70, 151.02, 156.20, 161.76, 162.52, 164.17, 192.76. ESI-MS (*m/z*): Calculated for $C_{29}H_{28}N_3O_4$ 483.22, found $[M+H]^+$ 484.46. Analysis calc. for

($C_{28}H_{27}N_3O_4$. 0.017 H_2O): C 72.03, H 6.04, N 8.69 %; found: C 72.33, H 6.11, N 8.71%.

2.4 Inhibition studies on acetylcholinesterase

The enzymatic activity was measured using an adaptation of the method previously described [19]. The assay solution contained 374 μL of (4-(2-hydroxyethyl)-1-piperazineethanesulfonic acid (Hepes) buffer (50 mM and pH 8.0), 476 μL of 5,5'-dithiobis-(2-nitrobenzoic acid) (DTNB, 3 mM), a variable volume (10-50 μL) of the stock solution of each compound in methanol (1 mg/mL), 25 μL of AChE (type VI-S, from electric eel) stock solution and the necessary amount of methanol to attain 0.925 mL of sample mixture in a 1 mL cuvette. The samples were left to incubate for 15 min and then 75 μL of acetylthiocholine iodide (AChI) solution (16 mM) was added. The reaction was monitored for 5 min at 405 nm. Assays were run with a blank containing all the components except AChE, which was replaced by Hepes buffer. The velocities of the reaction were calculated as well as the enzyme activity. A control reaction was carried out using the sample solvent (methanol) in the absence of any tested compound and it was considered as 100% activity. The percentage inhibition of the enzyme activity due to the presence of increasing test compound concentration was calculated by the following Eq. (1),

$$\%I = 100 - \left(\frac{v_i}{v_o} \times 100\right) \qquad (1)$$

in which v_i is the initial reaction rate in the presence of inhibitor and v_o is the initial rate of the control reaction. The inhibition curves were obtained by plotting the percentage of enzymatic inhibition versus inhibitor concentration and a calibration curve was obtained from which the linear regression parameters were obtained.

2.5 DPPH radical scavenging assays

The antioxidant activity was evaluated by 2,2-diphenyl-1-picrylhydrazyl (DPPH) radical scavenging activity assays previously described [24]. To a 2.5 mL solution of DPPH (0.002%) in methanol, four samples of each compound solution were added with different volumes to obtain different concentrations in a 3.5 mL final volume. The samples were incubated for 30 min at room temperature. The absorbance was measured

at 517 nm against the corresponding blank (methanol). The antioxidant activity was calculated by equation (2).

$$\%AA = -\frac{A_{DPPH} - A_{sample}}{A_{DPPH}} \qquad (2)$$

The tests were carried out in triplicate. The compound concentrations providing 50% of antioxidant activity (EC_{50}) were obtained by plotting the antioxidant activity against the compound concentration.

2.6 Solution equilibrium studies

2.6.1 Potentiometric and spectrophotometric studies

pH-potentiometric and UV-vis spectrophotometric titrations of compound **6** were accomplished in a 30% w/w DMSO/H_2O medium, at T = 25.0 ± 0.1 °C and ionic strength (I) 0.1 M KCl, by using 0.1 M KOH as titrant. Both glass and Ag/AgCl reference electrodes were previously conditioned in different DMSO/H_2O mixtures of increasing DMSO % composition and the response of the glass electrode was evaluated by strong acid – strong base (HCl/KOH) calibrations with the determination of the Nernst parameters by Gran's method [18]. The measurements were performed in a final volume of 20.00 mL, the ligand concentrations (C_L) were 1×10^{-3} M (potentiometry) and 2–3.75×10^{-5} M (spectrophotometry), under different C_M/C_L ratios: 0:1 (L), 1:1 (M/L, M = Fe, Cu, Zn), 1:2 (M/L, M = Cu, Zn) and 1:3 (Fe/L). The spectrophotometric measurements were carried out in a 250–500 nm wavelength range at pH ca 3–11. All titrations were performed in triplicate and under the stated experimental conditions the pK_w value (14.4) was determined and subsequently used in the computations. The stepwise protonation constant of the ligand, K = [HL]/[L][H], and the overall metal–complex stability constants, $\beta_{M_mH_hL_l} = [M_mH_hL_l]/[M]^m[H]^h[L]^l$, were calculated by fitting the pH-potentiometric and spectrophotometric data with, respectively, Hyperquad 2008 [25] and PSEQUAD programs [26]. The Fe(III) hydrolysis model was determined under the defined experimental conditions (I = 0.1 M KCl, 30% w/w DMSO/H_2O, T = 25.0 ± 0.1 °C) and the values of stability constants were log $\beta_{FeH_{-2}}$ = -6,78 and log $\beta_{FeH_{-3}}$ = -10,78; the Cu(II) and Zn(II) hydrolysis constants under the same experimental conditions (log $\beta_{Cu_2H_{-2}}$ = -9.94; log $\beta_{ZnH_{-2}}$ = -14.7, log $\beta_{ZnH_{-3}}$ = -22.08 [14]) were also

included in the fitting of experimental data towards the equilibrium models related to the Cu(II)/L and Zn(II)/L systems.

The species distribution curves were obtained with the Hyss program [25].

2.6.2 ESI-MS Spectra

The pH of the Fe(III)/**6** (C_L = 1.2 × 10^{-3} M), Cu(II)/**6** (C_L = 6 × 10^{-4} M) and Cu/**16** (C_L = 6 × 10^{-4} M) systems in aqueous solutions was previously ascertained to 4.04 and 6.01 (C_L/C_{Fe} = 3) as well as to 6.81 (C_L/C_{Cu} = 1 for **6**), 6.30 (C_L/C_{Cu} = 2 for **6**), 6.00 (C_L/C_{Cu} = 1 for **16**) and 6.60 (C_L/C_{Cu} = 2 for **16**) by using KOH solution, and the respective mass spectra were obtained from a LCQ Fleet mass spectrometer operated in the ESI positive and negative ion mode (Thermo Scientific). The optimized parameters were as following: ion spray voltage, +4.5 kV; capillary voltage, 16 V; tube lens offset, -63 V; sheath gas (N_2), 80 arbitrary units; auxiliary gas, 5 arbitrary units; capillary temperature, 250 °C. The spectra were recorded in the range 100 – 1000 Da. Spectra typically correspond to the average of 20–35 scans.

3. Results and Discussion

3.1 Molecular modeling studies of TAC-HBP hybrids

Docking studies of TAC-HBP hybrids into AChE, an enzyme involved in cholinergic loss, were performed in order to gain an insight into the type of interactions eventually established between this enzyme and the proposed inhibitors, therefore predicting the binding modes.

The active site of AChE contains a deep pocket where acetylcholine (substrate) can slip inside and be hydrolyzed into acetic acid and choline, that is no longer a neurotransmitter. The catalytic site of AChE is located near the bottom of that deep gorge and it is formed by three aminoacids, Ser200, His440 and Glu327 (sequence numbering of *Torpedo Californica* AChE, *Tc*AChE), known as the ‘catalytic triad’ of AChE [27]. There are still two main sites of binding for the AChE, one is located at the lower part of the gorge, formed by three important amino acids, Phe330, Trp84 and Glu199, and it is called as catalytic anionic site (CAS); the other, which is located at the entrance of the gorge and is formed by Trp279, Asp72 and Tyr70, is called as peripheral anionic site (PAS). Crystallographic structure has shown that the inhibitor tacrine binds

to CAS through π-stacking (with residues Trp84 and Phe330) and hydrogen-bonding interactions between its cyclic nitrogen and His440 [28]. While its aromatic aminoquinoline moiety is largely responsible for the binding to AChE, the cyclohexyl portion is related with the blocking of ACh approach to the active site.

The strategy followed herein for the design of new potential anti-AD drugs was the coupling of two main moieties – tacrine (TAC) and hydroxybenzoyl-pyridone (HBP) - through an alkyl spacer, which selection was aided by the screening of the envisioned TAC-HBP hybrids against AChE. It is well recognized that compounds which are able to interact with both CAS and PAS are good AChE inhibitors. Therefore, the length of the alkyl spacer between the selected two moieties in the proposed inhibitors has been decided by the docking study performed with program GOLD, v. 5.1 [29], in order to assure that one moiety can interact with CAS while at the same time the other moiety is able to interact with PAS and so attain maximum AChE inhibition.

The crystal structure of *Tc*AChE complexed with an inhibitor was taken from RCSB Protein Data Bank (PDB, entry 1ODC) [30]. This structure was chosen due to the similarity found between its inhibitor and the herein designed ligands. In fact, the original ligand (*N*-quinolin-4-yl-*N´*-(1,2,3,4-tetrahydroacridin-9-yl)octane-1,8-diamine) contains a tacrine moiety connected through a long carbon chain to an amino-quinoline group, which is structurally very similar to the HBP moiety. The docking calculations were performed using the ASP scoring function, since this function has previously proved to give the best docking predictions for AChE inhibitors [13,31]. For each compound, one conformation was selected to give a good compromise between the best consensus score and that with the closest alignment to the original ligand.

The molecular modelling studies revealed favorable interactions for three proposed compounds (**15**-**17**, see Fig. 2), which present many similarities in their binding conformations. Actually, Fig. 2 shows that the three designed ligands are well inserted into the cavity of the active site, blocking the entrance to the substrate (choline) and water molecules. The tacrine moiety is always found completely implanted close to the bottom of the gorge of the enzyme, binding to the CAS by π–π stacking with the aromatic ring of Trp84 and Phe330 (as in tacrine crystallographic structure), and overlapping almost perfectly with the tacrine moiety of the original ligand. On the other way, both the alkyl spacer and the pyridone ring seem to be well accommodated along the hydrophobic cavity, while the benzoyl ring of the designed inhibitors is always placed at the entrance of the gorge, being able to bind with PAS through aromatic

stacking with Tyr70 and Trp279. Interestingly, compound **17**, which has an alkyl spacer of four methylene carbon atoms, establishes a further favorable H-bond between the OH group of the benzoyl ring attached to the HBP moiety and ASP275 residue. In the case of compounds **15** and **16**, which have an alkyl spacer of two methylene units, there is no hydrogen bond formation with ASP275, probably due to the smaller chain size but also to the fact that these compounds contain one methoxy and one hydroxy groups instead of two hydroxy groups as in **17**. Overall, the docking into AChE of the designed compounds (**15**-**17**) suggests their ability to interact with both the CAS and PAS, therefore being able to act as dual-binding site AChE inhibitors, which is undoubtedly encouraging to pursuit their synthesis and evaluation as potential multifunctional anti-AD drugs.

Fig. 2 - Docking of TAC-HBP hybrids into AChE: superimposition of **15** (violet), **16** (light green) and **17** (pink) with original ligand *N*-quinolin-4-yl-*N*'-(1,2,3,4-tetrahydroacridin-9-yl)octane-1,8-diamine (yellow). H-bond is represented as a solid sky-blue line.

3.2 Synthesis of the compounds

All the designed HBP derivatives (**6**-**8**) and TAC-HBP hybrids (**15**-**17**) have been synthesized from the (*E*)-ethyl-3-(4-oxo-4*H*-chromen-3-yl) acrylates (**3**-**5**) and coupling of free amino alkyl substituted HBP derivatives (**12**-**14**) with 9-chloro-1,2,3,4-tetrahydroacridine (**2**), respectively (Scheme). The key intermediates **3**-**5** were first synthesized by following the literature procedure [16], which, from reaction with various alkylamines and *t*-butyl(2-aminoethyl)carbamate in ethanol under catalytic amount of triethylamine, gives the desired compounds (**6**-**8**) and intermediates **9**-**11** under a three-step addition-elimination and rearrangement sequence in one pot. The free amino alkyl substituted HBP derivatives (**12**-**14**) were then obtained by the acid hydrolysis of the carbamate group from **9**-**11**. Finally, the coupling of **12**-**14** with **2** (synthesized from literature procedure [19]) in the presence of phenol and a catalytic amount of potassium iodide under reflux gave the desired TAC-HBP conjugates **15**-**17** (Scheme).

Scheme - Synthesis of HBP derivatives. Reagents and conditions: a) cyclohexanone, $POCl_3$, 180 ^oC, 4 hr; b) R^1NH_2 (1.05 eq), NEt_3 (1-2 drops), C_2H_5OH, reflux, 8-10 h; c) DCM, TFA, 7-8 hr; d) Phenol, KI, 165-170 ^oC 15 min.

3.3 Acetylcholinesterase inhibitory activity

The AChE inhibitory activities of the newly synthesized TAC-HBP conjugates (**15**-**17**), as well as of the model compound **6**, were evaluated by adaptation of the spectroscopic method described by Ellman [13]. The IC_{50} values for AChE inhibition are summarized in Table 1. As expected from molecular docking, all of the three designed conjugates display high inhibitory activities against this enzyme, with IC_{50} values lying in the sub-micromolar range. Out of the three evaluated hybrids, conjugate **17** appears to be the strongest inhibitor, with IC_{50} value of 0.57 µM, quite close to the value obtained for tacrine (IC_{50} = 0.31 µM), followed by **16** and **15** with IC_{50} values of 0.71 and 0.78 µM respectively. The HBP derivative **6** exhibited AChE inhibition at significantly higher concentration (IC_{50} = 840 µM), thus demonstrating the protagonist role of the tacrine moiety in the enzyme inhibition of the developed tacrine hybrids. Moreover, the structure–activity analysis of these compounds allows concluding that the inhibitory potency against AChE is closely related with the length of the linker between the two coupled moieties. In fact, analysis of the results suggests that compound **17**, containing a four methylene unit's linker between tacrine and HBP, seems to provide a suitable length to fit comfortably between CAS and PAS site of enzyme, allowing the establishment of a H-bond between an OH group of the benzoyl ring in the HBP moiety and ASP275 residue in the PAS as already seen from the docking studies, which explains its better AChE inhibitory activity than **15** and **16** with shorter chain lengths and unable to form H-bonding. Although GOLD program used in the present work is not able to determine the ligand – protein binding energy and only three experimental points were obtained herein, it was tentatively established a correlation between the fitness score values of GOLD, resulting from the docking of each compound (**15**-17), and the experimentally obtained IC_{50} values. A good linear correlation (R^2 = 0.9947, see Fig. S13 in Supplementary Information) was observed, evidencing some potential correspondence between the fitness of the compounds to the enzyme and their respective inhibitory activity.

Table 1 – Inhibitory activity (IC_{50}, μM) of AChE and DPPH radical scavenging capacity (EC_{50}, μM) for the studied compounds, tacrine and huperzine A.

The new developed tacrine hybrids appear to have a slightly lower capacity to inhibit AChE then the reference drugs, tacrine and the racemic mixture **(±)**-HupA [33], but they are expected to exhibit additional properties, such as antioxidant activity and metal chelating capacity provided by the HBP moiety, which will make them promising candidates for the multi-target combat of Alzheimer´s disease.

3.4 In vitro free radical scavenging activity

Antioxidants are considered valuable therapeutic tools in the prevention or therapy of AD since there is evidence that AD brains exhibit oxidative injury in several classes of cellular macromolecules [34].

Therefore, a series of six selected compounds, namely three HBP derivatives (**6**-**8**) and three TAC-HBP conjugates (**15**-**17**), was herein screened for their DPPH radical scavenging capacity (EC_{50}) [24] and the corresponding results are summarized in Table 1. Analysis of the experimental data obtained shows that, among the HBP derivatives (**6**-**8**), the 2′,5′-dihydroxybenzoyl substituted compound **8** was found to exhibit an exceptional good antioxidant activity (EC_{50} = 4.28 μM), even better than the value found by the same method for vitamin C (EC_{50} = 15 μM [35]), followed by the 2′,4′-dihydroxybenzoyl substituted derivative **7** with EC_{50} value of 95 μM. Interestingly, although both compounds **7** and **8** carry the same number of hydroxyl groups (two) on the benzoyl ring, they show a huge difference in antioxidant activity. The much higher activity of compound **8** in comparison with **7** can be explained by the fact that the former is able to release hydrogen for DPPH quenching more easily than the later one due to the possible formation of a stable 1,4-quinone. Furthermore, as already expected, the substitution of one hydroxyl group of **7** by a methoxy unity (compound **6**) is responsible for an accentuated decrease (ca 2-fold) in radical scavenging capacity.

The analysis of the DPPH radical scavenging activity data for the TAC-HBP conjugates (**15**-**17**) shows that even though their activity is lower than that of the HBP compounds, the found DPPH radical scavenging capacity is much improved when compared with that of the parent drug tacrine (EC_{50} > 1000 μM). Moreover, the radical scavenging

activity screening of these TAC-HBP conjugates suggests that the 2′,4′-dihydroxy substituted conjugate **17** exhibits a higher potential (EC_{50} = 204 μM) than the 2′-hydroxy -4′/5′-methoxy substituted conjugates **15-16** (EC_{50} 213-249 μM), according with the results obtained for the HBP compounds. So, as a conclusion, it can be stated that HBP moieties are successful in bringing antioxidant activity to hybrids **15-17** which have been synthesized from a non-active tacrine.

3.5 Metal chelating capacity

Research on neurodegenerative diseases has also been dealing with metal chelation, due to the general recognition that chelators interfere not only in metal-induced Aβ aggregation and neurotoxicity but also on metal homeostasis of AD brains. Since the herein studied tacrine derivatives **15-17** have a common 2-hydroxybenzoyl chelating core, compound **6**, a 2′-hydroxy-4′-methoxybenzoyl-2-pyridinone derivative, was chosen as a model to analyze their chelating capacity towards redox-active (Fe(III), Cu(II)) and Aβ-binding (Cu(II), Zn(II)) metal ions. Due to solubility reasons, these equilibrium solution studies were accomplished in a mixed 30% (w/w) DMSO/water medium, In fact, DMSO was chosen because it is a quite used and well tolerated solvent in biological and cellular studies, the amounts of ligand (< 7 μM) and DMSO (< 1%) employed in culture media being quite low with concomitant no alterations observed in cells [13,36].

Firstly, the protonation constant (log *K*) of **6**, corresponding to the phenolic hydroxyl group, was determined by pH-potentiometric as well as ultraviolet-visible (UV-vis) spectrophotometric titrations (see Fig. 3) reaching identical values (see Table 2). Nevertheless, in the following calculations for the metal/**6** systems, the log *K* value obtained by each experimental method will be used in the complexation studies performed by the same methodology.

Fig. 3 - a) pH-potentiometric titration curves of **6** (C_L = 1 × 10^{-3} M); b) Spectrophotometric absorption spectra of **6** recorded for 3.68 < pH < 11.05 (C_L = 2 × 10^{-5} M) and inset containing the individual calculated spectra by PSEQUAD.

Table 2 - Protonation constant of model compound **6**, global formation constants[a] of its metal (Fe(III), Cu(II), Zn(II)) complexes (T = 25.0 ± 0.1 °C, I = 0.1 M KCl, 30% w/w DMSO/water) and pM[b] values as well as for other selected bidentate chelators.

Compound **6** was obtained in the neutral monoprotonated form (HL). The inset of Fig. 3 b), containing the calculated spectra (PSEQUAD) of the mono- and deprotonated forms of this compound, as well as Fig. 4, prove that the maximum at 297 nm corresponds to both species (HL and L) while that at 383 nm belongs only to the deprotonated L form.

Fig. 4 - Species distribution curves for **6** with molar extinction coefficients at the maximum absorption wavelengths ($C_L = 2 \times 10^{-5}$ M).

Although compound **6** contains a hydrophilic OH group, at the physiological pH (7.4) and for $C_L = 10^{-5}$ M it is mainly in the neutral HL form (97.5%), thus reflecting a low hydrophilicity and the need to use a 30% DMSO/water medium in solution studies. The high value of the protonation constant of **6** (ca 9) reflects the stabilization of the protonated HL species resulting from the establishment of an intramolecular H-bond between the phenolic hydroxide (H-bond donor) and the *O*-ketone (H-bond acceptor). Besides stabilizing the enol form of the phenol group, there is also a conjugation effect with the double bond of the ketone group. In fact, this has also been observed (in aqueous medium) for 2-acetylphenol (log K = 9.87) when compared to its analogue 4-acetylphenol (log K = 8.05) [37].

The chelating ability of compound **6** towards the three metal ions under study – Fe(III), Cu(II) and Zn(II) - was evaluated through the determination of the global formation constants of the complexes by pH-potentiometric (Hyperquad 2008 program [24]) titrations and also for the Fe(III) complexes by UV-vis spectrophotometry (PSEQUAD program [25]). From Fig. 2 a) it is possible to observe that for all the metal ions under study there is a large change in the deprotonation profile of the ligand titration curve due to the presence of the metal ion. Actually, all the curves of the metal/**6** systems lye below that of the ligand for $0 < a < 1$, therefore evidencing the formation of metal complexes with the deprotonated form of the ligand (L) with relative stability order Fe > Cu > Zn. These results point towards a β-phenol-keto coordination mode, with

formation of 6-membered rings, such as already found for the Co(II), Ni(II) and Cu(II) complexes of salicylaldehyde [43].

As stated above for the Fe(III)/**6** system, both pH-potentiometric and spectrophotometric titrations were performed for the 1:1 and 1:3 Fe(III)/ligand molar ratios, although the complexation model presented in Table 2 and used in Fig. 5 a) for the 1:3 system corresponds to the one obtained by spectrophotometry since at the beginning of potentiometric titration (C_L = 1 × 10^{-3} M) both FeL and FeL_2 coexisted with *ca* 80% FeL.

Fig. 5 – a) Species distribution curves for the 1:3 Fe(III)/**6** system with molar extinction coefficients at the maximum absorption wavelengths (C_L = 3.75 × 10^{-5} M); b) Spectrophotometric absorption spectra of **6** (pH = 7.80, C_L = 2 × 10^{-5} M) and Fe(III)/**6** 1:3 (pH = 6.44, C_L = 3.75 × 10^{-5} M).

From the spectra obtained for the 1:1 Fe(III)/**6** system, β_{FeL} was calculated and the stability constants of the remaining complex species were determined from the titration performed under 1:3 molar stoichiometry of metal ion to ligand while holding the value of β_{FeL} constant. Fig. 5 a), containing the species distribution curves for the 1:3 Fe(III)/**6** system, shows that at the used experimental conditions, the iron complexation begins below pH 3, with the formation of both FeL and FeL_2 complexes, while FeL_3 is predominant above pH ca 4.5 (78% of FeL_3 at pH 7.4 and micromolar metal concentration - C_L = 10 × C_M), therefore confirming the expected good chelating power of compound **6** toward Fe(III).

All the iron complex species formed have identical absorption maximum at *ca* 296 nm up to pH 8, but above that value another band appears at 386 nm corresponding to the deprotonated ligand (Fig. 5 a)). The superposition of UV-vis spectra of Fe(III)/**6** (pH = 6.44) and **6** (see Fig. 5 b)) reveals that the coordination of the Fe(III) ion is responsible for an high increase in the intensity of the band at 296 nm for the complex although no shift of this band is observed.

Both studies of Cu(II) and Zn(II) complexation with compound **6** were performed by potentiometric titration and the respective species distribution curves for the 1:2 Cu(II)/**6** and 1:1 Zn(II)/**6** systems at the used experimental conditions are shown in Fig.5. For the 1:1 and 1:2 Cu(II)/**6** systems precipitation occurred above ca pH 6,

probably due to the formation of insoluble hydroxocomplexes, while for the Zn(II)/**6** systems no precipitation was observed. It is also possible to see that, at the concentrations used in the experimental conditions, complexation of Cu(II) and Zn(II) begins above pH 4 and 5.5, respectively (see Fig. 6), and that a strong competition exists with metal hydroxide species.

Fig. 6 - a) Species distribution curves for the 1:2 Cu(II)/**6** and b) 1:1 Zn(II)/**6** systems ($C_L = 1 \times 10^{-3}$ M).

ESI-MS data was also obtained for solutions of Fe(III)/**6** and Cu(II)/**6** in 1:3 (Fe/L), 1:1 (Cu/L) and 1:2 (Cu/L) stoichiometric conditions and at convenient pH values (see Experimental part). These spectra confirmed the existence of 1:1 and 1:3 iron complexes, respectively, as $[Fe(HL)Cl_2]^+$, $[FeL(HL)_2Cl]^+$ and $[FeL_3Cl]^-$; regarding the copper complexes, 1:1 species, such as $[Cu(HL)Cl]^+$, as well as polymeric species $[Cu_2L_3]^+$ were found, the last one in a higher quantity for the 1:2 metal/ligand molar ratio stoichiometric conditions (see Table 3). Under the experimental conditions of ESI/MS it was not possible to observe the formation of the CuL_2 complex, possibly owing to its low percent formation and also to some precipitation of hydroxo species.

Table 3 - ESI-MS ions for the Fe(III) and Cu(II) complexes of **6** in aqueous solution (1:3 Fe/L, $C_L = 1.2 \times 10^{-3}$ M; 1:1 and 1:2 Cu/L, $C_L = 6 \times 10^{-4}$ M).

Comparison of the metal chelating capacity of compound **6** with that of some selected bidentate analogous chelators (see Table 2), namely salicylaldehyde and 2-acetylphenol, allows to conclude that the values of the corresponding global stability constants tend to be analogous, even though different solution media and ionic strengths were used. In fact, it is not easy to establish an accurate comparison since, in some cases, pM values in Table 2 were determined by using different metal hydrolysis models (2-acetylphenol) or were not determined (salicylaldehyde with $I = 0.5$ M), while in other cases (salicylaldehyde, 2-acetylphenol) the model for the Fe(III)/L systems was incomplete for the medium solution conditions chosen with corresponding decrease of pFe values. Since precipitation occurred above pH 6 in the case of Cu(II)/**6** systems, that pH value was chosen to determine all the pM values corresponding to compound **6** (see Table 2). Nevertheless, when comparing the calculated pFe and pZn values for **6** at

pH 7.4 (pFe = 18.1, pZn = 6.5), to simulate physiological conditions, with those of a well known strong iron chelator, deferiprone (DFP), at the same pH value (pFe = 19.4 - 20.7, pZn = 6.2) it is possible to infer that compound **6** is a good iron chelator, although weaker than DFP. These values reflect two features working in opposite direction: the fact that 6-membered chelate rings are involved in the complexes of **6**, against more favorable 5-membered ones in those of DFP; also the fact that a 30% w/w DMSO/H_2O medium can increase the values of stability constants relative to an aqueous medium, due to the relative balance established between electrostatic and non electrostatic forces for media with different dielectric constants [44].

Besides evaluating the chelating capacity of the HBP moiety with model compound **6**, the chelating ability of the TAC-HBP hybrids was also confirmed by UV-vis spectrophotometry and ESI-MS spectrometry with compound **16**. Actually, Fig 7 shows an increase in the intensity of the UV bands when copper is coordinated to compound **16**, similarly to previously observed for **6** and Fe(III) (see Fig. 5b)); also, the presence of 1:2 (Cu/L) complexes, as $[CuL_2H]^+$ and $[Cu(HL)_2Cl]^+$ (see Table 3), was confirmed by ESI-MS. Unfortunately, for the system Cu(II)/**16**, under the experimental conditions of ESI/MS, it was not possible to observe the formation of the CuL complex.

Fig. 7 – a) Spectrophotometric absorption spectra of **16** and Cu(II)/**16** 1:2 (pH = 7.40, $C_L = 2 \times 10^{-5}$ M); b) Expanded ESI(+) mass spectrum of Cu(II)/**16** 1:1 (pH=6.00, $C_L = 6 \times 10^{-4}$ M) showing a group of peaks at *m/z* 999.8 /1001.9 attributed to $[CuL_2H]^+$ species. The inset presents the calculated isotopic pattern for the cation $[C_{56}H_{53}CuN_6O_8]^+$.

In this section it has been proved that 5-(2-hydroxybenzoyl)-pyridin-2(1*H*)one moieties are moderate/good chelators of Fe(III), Cu(II) and Zn(II) and that by including them in the design of potential anti-AD drugs their chelating capacity towards that well-known triad of transition metal ions can be assured.

3.6. Molecular modeling of the 1:3 Fe(III)/6 complex

In the absence of X-ray structures for the metal complexes of model compound **6**, a molecular modelling study was accomplished to show the 1:3 Fe(III)/**6** iron complex

structure. This study was carried out with full geometry optimization of the ligand and respective Fe(III) complex by quantum mechanical calculations based on density functional theory (DFT) methods [45] included in the Gaussian 03 program software [46] with the B3PW91 functional [47]. Geometry optimizations were obtained by using 3-21G basis set [48] for all elements, first, and afterwards re-optimized using 6-31G** [49] for the main group elements and the Stuttgart–Dresden pseudopotential (SDD) and associated basis set for Fe [50]. No symmetry constrains were enforced during geometry optimizations.

Fig. 8 – DFT-minimized structure of the FeL_3 complex of compound **6**. Coloring of atoms: Fe turquoise, N blue, O red, C grey and H white.

The energy-minimized structure obtained for complex FeL_3 of compound **6** confirms a β-phenol-keto metal coordination core for each ligand, with a slightly distorted octahedral geometry entirely composed by hard oxygen donor atoms (see Fig. 8). In fact, coordination bond distances are somehow higher for Fe-O_{keto} (1.925-1.946 Å) than for Fe-O_{phenol} (1.871-1.896 Å) and also bond angles involving the hard iron metal ion (O-Fe-O) tend to be slightly higher within the hexadentate chelating ring of each ligand (89.0-92.2 ^{0}C) than between different ligands (89.4-90.2 ^{0}C). These parameters reveal that the keto oxygen atoms are less strained than the phenolic ones therefore compensating the relatively more rigid phenolic donor atoms and allowing a good accommodation of the metal ion in the coordination shell.

1. Conclusions

Tacrine-(hydroxybenzoyl-pyridone) (TAC-HBP) hybrids were designed by conjugating an active AChE inhibitor (tacrine) with a 2-hydroxybenzoyl-2-pyridone (HBP) moiety through an alkyl chain with adequate length capable to assure dual-binding mode of enzyme inhibition. After preliminary docking studies, three TAC-HBP conjugates (**15-17**) were selected to be synthesized, biologically evaluated for AChE inhibition and also assayed for radical scavenging activity (DPPH method). Screening results showed that all the compounds display inhibitory activities close to tacrine, with IC_{50} values lying in the sub-micromolar range (0.57-0.78 μM), and exhibit good antioxidant activity (EC_{50} = 204-249 μM) conferred by the HBP moiety. The higher anti-AChE activity of

compound **17** (IC_{50} = 0.57 μM) confirms the possible better fitting of this compound between CAS and PAS as well as its capacity for H-bonding as previewed by molecular modelling studies. Finally, the chelating capacity of the developed tacrine hybrids was evaluated by studying the complexation ability of a 2′-hydroxy-4′-methoxybenzoyl-2-pyridinone derivative (compound **6**), as a model compound, towards three redox-active and/or Aβ-binding metal ions (Fe(III), Cu(II)), Zn(II)) by using potentiometric, UV-vis spectrophotometric and ESI-MS techniques. It was proved that the HBP moiety acts as a moderate/good chelator of these metal ions (pFe = 13.9, pCu = 6.0 and pZn = 6.0 at pH 6.0, C_L/C_M = 10, C_M = 10^{-6} M), being able to form complexes of variable maximum metal/ligand stoichiometry: 1:3 for Fe(III), 1:2 for Cu(II) and 1:1 for Zn(II). Molecular modelling of the 1:3 iron complex of model compound **6** showed an octahedral coordination around the iron(III) metal ion, involving a β-phenol-keto coordination mode. UV and ESI-MS spectra for the system Cu(II)/**16** proved that the hybrids are also able to chelate metal ions. In the search for multifunctional anti-Alzheimer's disease drugs, the performed work evidenced the importance of conjugating these two main moieties. In fact, the resulting tacrine conjugates are dual-binding site AChE inhibitors, with anti-AChE activity comparable to the parent compound tacrine, but further showing antioxidant capacity and biometal chelation ability conferred by the HBT moiety.

Abbreviations

Aβ	amyloid-β
ACh	acetylcholine
AChE	acetylcholinesterase
AChI	acetylthiocholine iodide
AD	Alzheimer´s disease
BuChE	butyrylcholinesterase
CAS	catalytic anionic site
ChEIs	cholinesterase inhibitors
COSY	correlation spectroscopy
DCM	dichloromethyl
DFP	deferiprone
DFT	density functional theory
DNA	deoxyribonucleic acid
DPPH	2,2-diphenyl-1-picrylhydrazyl
DTNB	5,5'-dithiobis-(2-nitrobenzoic acid)
ESI-MS	electrospray ionization-mass spectrometry
HBP	hydroxybenzoyl-pyridone
Hepes	4-(2-hydroxyethyl)piperazine-1-ethanesulfonic acid
HSQC	heteronuclear single quantum coherence spectroscopy
HupA	Huperzine A
MTDLs	multi-target-directed ligands
PAS	peripheral anionic site
ROS	reactive oxygen species
RT	room temperature
SDD	Stuttgart–Dresden pseudopotential
TAC	tacrine
TFA	trifluoracetic acid
TLC	thin layer chromatography
UV-vis	ultraviolet-visible spectrophotometry

Acknowledgments

The authors thank the Portuguese NMR (IST-UL Center) and Mass Spectrometry Networks (Node IST-CTN) for providing access to their facilities, as well as to Dr. Maria da Conceição Oliveira for helping in the interpretation of ESI-MS data. Financial support is acknowledged to the Portuguese Foundation of Science and Technology (FCT) for Project UID/QUO/ 00100/2013 and fellowship to K.C. H.M.A. is thankful to Erasmus Mundus ACTION2 Program (WELCOME Scholarship WELC1104289).

References

[1] R. Jakob-Roene, H. Jacobsen, Angew. Chem. Int. Ed. 48 (2009) 3030-3059.

[2] E. Scarpini, P. Scheltens, H. Feldman, Lancet Neurol. 2 (2003) 539-547.

[3] L.M. Sayre, G. Perry, M.A. Smith, Chem. Res. Toxicol., 21 (2008) 172–188.

[4] C.G. Ballard, Eur. Neurol. 47 (2002) 64-70.

[5] E. Giacobini, Neurochem. Int. 32 (1998) 413-419.

[6] R. León, A.G. Garcia, J. Marco-Contelles, Med. Res. Rev., 33 (2013) 139-189.

[7] A. Nunomura, G. Perry, G. Aliev, K. Hirai, A. Takeda, E.K. Balraj, P. K. Jones, H. Ghanbari, T. Wataya, S. Shimohama, S. Chiba, C.S. Atwood, R.B. Petersen, M.A. Smith, J. Neuropathol. Exp. Neurol. 60 (2001) 759-767.

[8] X.D. Huang, R.D. Moir, R.E. Tanzi, A.I. Bush, J.T. Rogers, Ann. N. Y. Acad. Sci. 1012 (2004) 153-163.

[9] A.P. Kozikowski, G. Campiani, L.-Q. Sun, S. Wang, A. Saxena, B.P. Doctor, J. Am. Chem. Soc. 118 (1996) 11357-11362.

[10] X. Sui, C. Gao, Int. J. Mol. Med. 33 (2014) 227-233

[11] M.E. Wall, Med. Res. Rev. 18 (1998) 299-314.

[12] M. Torres, S. Gil, M. Parra, Curr. Org. Chem. 9 (2005) 17-54757-1779.

[13] A. Nunes, S.M. Marques, C. Quintanova, D.F. Silva, S.M. Cardoso, S. Chaves, M.A. Santos, Dalton Trans 42 (2013) 6058-6073.

[14] C. Quintanova, R.S. Keri, S. Chaves**,** M.A. Santos, J. Inorg. Biochem. 151 (2015) 58-66.

[15] R.S. Keri, C. Quintanova, S. Chaves, D.F. Silva, S.M. Cardoso, M.A. Santos, Chem. Biol. Drug Des. 87 (2016) 101-111.

[16] C. Karam, S. Prasad, K. Rakesh, R.K. Tiwari, A.N. Shirazi, S. Kumar, K. Parang, S.K. Sharma, Bioorg. Chem. 53 (2014) 75-82.

[17] W.L.F. Armarego, D.D. Perring (Eds) Purification of laboratory chemicals, Butterworth–Heinemann Press, 4th ed, Oxford, 1999.

[18] F.J.C. Rossotti, H. Rossotti, J. Chem. Ed. 42 (1965) 375-378.

[19] R.S. Keri, C. Quintanova, S.M. Marques, S.M. Cardoso, M.A. Santos, Bioorg. Med. Chem. 21 (2013) 4559-4569.

[20] Maestro, version 9.3. Schrödinger Inc.: Portland, OR, 2012.

[21] T. Hassinen, M. Peräkylä, J. Comput. Chem. 22 (2001) 1229-1242.

[22] G. Jones, P. Willett, R.C. Glen, A.R. Leach, R. Taylor, J. Mol. Biol. 267 (1997) 727-748.

[23] K. Chand, A.K. Sharma, S.K. Sharma, Magn. Reson. Chem. 54 (2016) 91-102.

[24] B. Tepe, D. Daferera, A. Sokmen, M. Sokmen, M. Polissiou, Food Chem. 90 (2005) 333-340.

[25] P. Gans, A. Sabatini, A. Vacca, Talanta 43 (1996) 1739-1753.

[26] L. Zékány, I. Nagypál, G. Peintler, PSEQUAD version 5.01, 2001.

[27] H. Dvir, I. Silman, M. Harel, T.L. Rosenberry, J.L. Sussman, Chem-Biol. Interact. 187 (2010) 10–22.

[28] M. Harel, I. Schalk, L. Ehret-Sabatier, F. Bouet, M. Goeldner, C. Hirth, P.H. Axelsen, I. Silman, J.L. Sussman, Proc. Natl. Acad. Sci. U. S. A. 90 (1993) 9031-9035.

[29] G. Jones, P. Willett, R.C. Glen, A.R. Leach, R. Taylor, J. Mol. Biol., 267, (1997) 727-748.

[30] Protein Data Base (PDB). http://www.pdb.org/pdb/home/home.do

[31] J. Sebestik, S.M. Marques, P.L. Fale, S. Santos, D.M. Arduino, S.M. Cardoso, C.R. Oliveira, M.L. Serralheiro, M.A. Santos, J. Enzyme Inhib. Med. Chem. 26 (2011) 485-497.

[32] X. Chao, X. He, Y. Yang, X. Zhou, M. Jin, S. Liu, Z. Cheng, P. Liu, Y. Wang, J. Yu, Y. Tan, Y. Huang, J. Qin, S. Rapposelli, R. Pi, Bioorg. Med. Chem. Lett. 22 (2012) 6498–6502.

[33] X.C. Tang, G.H. Kindel, A.P. Kozikowski, I. Hanin, J. Ethnopharmacol. 44 (1994) 147–155.

[34] D. Pratico, Trends Pharmacol. Sci. 29 (2008) 609-615.

[35] Y. Zhao, J. Dou, T. Wu, H.A. Aisa, Molecules,18 (2013) 951-962.

[36] S.M. Marques, C.C. Abate, S. Chaves, F. Marques, I. Santos, E. Nuti, A. Rossello, M.A. Santos, J. Inorg. Biochem. 127 (2013) 188–202.

[37] A.E. Martell, R.M. Smith, Critical Stability Constants, Vol. 3, Plenum Press, New York and London, 1977.

[38] R.M. Smith, A.E. Martell, Critical Stability Constants, Vol. 4, Plenum Press, New York and London, 1976.

[39] Z.D. Liu, R.C. Hider, Coord. Chem. Rev. 232 (2002) 151-171.

[40] V.M. Nurchi, G. Crisponi, T. Pivetta, M. Donatoni, M. Remelli, J. Inorg. Biochem. 102 (2008) 684-692.

[41] E.T. Clarke, A.E. Martell, Inorg. Chim. Acta 191 (1992) 57-63.

[42] M.A. Santos, S.M. Marques, S. Chaves, Coord. Chem. Rev. 256 (2012) 240-259.

[43] G.C. Percy, D.A. Thomton, J. Inorg. Nucl. Chem. 35 (1973) 2719-2726.

[44] S. Raju, K.B.K. Naik, B.A. Kumar, G.N. Rao, J. Ind. Chem. Soc. 89 (2012) 57-62.

[45] R.G. Parr, W. Yang, Density Functional Theory of Atoms and Molecules, Oxford University Press, New York, 1989.

[46] Gaussian 03, Revision C.02, M.J. Frisch, G.W. Trucks, H.B. Schlegel, G.E. Scuseria, M.A. Robb, J.R. Cheeseman, J. A. Montgomery, Jr., T. Vreven, K.N. Kudin, J.C. Burant, J.M. Millam, S.S. Iyengar, J. Tomasi, V. Barone, B. Mennucci, M. Cossi, G. Scalmani, N. Rega, G.A. Petersson, H. Nakatsuji, M. Hada, M. Ehara, K. Toyota, R. Fukuda, J. Hasegawa, M. Ishida, T. Nakajima, Y. Honda, O. Kitao, H. Nakai, M. Klene, X. Li, J.E. Knox, H.P. Hratchian, J.B. Cross, V. Bakken, C. Adamo, J Jaramillo, R. Gomperts, R.E. Stratmann, O. Yazyev, A.J. Austin, R. Cammi, C. Pomelli, J.W. Ochterski, P.Y. Ayala, K. Morokuma, G.A. Voth, P. Salvador, J.J. Dannenberg, V.G. Zakrzewski, S. Dapprich, A.D. Daniels, M.C. Strain, O. Farkas, D.K. Malick, A.D. Rabuck, K. Raghavachari, J.B. Foresman, J.V. Ortiz, Q. Cui, A.G. Baboul, S. Clifford, J. Cioslowski, B.B. Stefanov, G. Liu, A. Liashenko, P. Piskorz, I. Komaromi, R.L Martin, D.J. Fox, T. Keith, M.A. Al-Laham, C.Y. Peng, A. Nanayakkara, M. Challacombe, P.M.W. Gill, B. Johnson, W. Chen, M.W. Wong, C. Gonzalez, J.A. Pople, Gaussian, Inc., Wallingford CT, 2004.

[47] J.P. Perdew, K. Burke, Y. Wang, Phys. Rev. B 54 (1996) 16533-16539.

[48] K.D. Dobbs, W.J. Hehre, J. Comp. Chem. 8 (1987) 861-879.

[49] P.C. Hariharan, J.A. Pople, Theor. Chim. Acta 28 (1973) 213-222.

[50] T. Leininger, A. Nicklass, H. Stoll, M. Dolg, P. Schwerdtfeger, J. Chem. Phys. 105 (1996) 1052–1059.

Table 1 – Inhibitory activity (IC_{50}, μM) of AChE and DPPH radical scavenging capacity (EC_{50}, μM) for the studied compounds, tacrine and huperzine A.

Compound	EeAChE (IC_{50}, μM)[a]	DPPH scavenging (EC_{50}, μM)[b]
6	840 ± 3	178 ± 2
7	nd[c]	95 ± 2
8	nd[c]	4.28 ± 0.06
15	0.78 ± 0.01	249 ± 2
16	0.71 ± 0.03	213 ± 2
17	0.57 ± 0.05	204 ± 2
tacrine	0.31 ±0.02	> 1000[d]
(±) Hup A	0.3[e]	-

[a] mean ± SEM (standard error of the mean) of 3 experiments for 50% inhibition of electric eel AChE (EeAChE); [b] mean ± SD of 3 independent experiments for 50% antioxidant activity; [c] not determined; [d] ref. 32; [e] rat brain, ref. 33.

Table 2 – Protonation constant of model compound **6**, global formation constants[a] of its metal (Fe(III), Cu(II), Zn(II)) complexes (T = 25.0 ± 0.1 °C, I = 0.1 M KCl, 30% w/w DMSO/water) and pM[b] values as well as for other selected bidentate chelators.

Compound	log K_i	$M_mH_hL_l$	log $\beta_{Fe_mH_hL_l}$	log $\beta_{Cu_mH_hL_l}$	log $\beta_{Zn_mH_hL_l}$
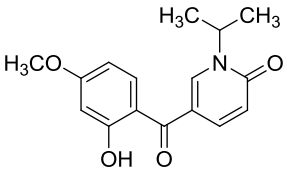 **6**	Pot 8.97(1) Spect 8.99(1)	(011) (101) (102) (1-11) (011) (101) (102) (103) **pM**	 12.16(5) 22.56(2) 32.12(5) **13.9**	6.11(5) 12.08(5) - **6.0**	4.61(5) - -2.69(2) **6.0**
 Salicylaldehyde[c]	8.07	(011) (101) (102)	 8.75 15.55	 5.36 10.11	 2.87 5.00
 2-acetylphenol[d]	9.87	(011) (101) (102) **pM**[e]	 10.52 - **11.3**	 6.49 11.74 **6.0**	 -
 DFP	9.77[f] 9.82[g] 3.62[f] 3.66[g]	(011) (021) **pM**[h]	 **19.4**; **20.7**	 **10.5**	 **6.2**

[a] $\beta_{M_mH_hL_l} = [M_mH_hL_l]/[M]^m[H]^h[L]^l$; [b] pM = −log[M] with C_L/C_M = 10 and $C_M = 10^{-6}$ M at pH 6.0: [c] I=0.5 M (ref. 37) and so pM values were not determined; [d] ref. 37; [e] pM values determined with metal hydrolysis constants in aqueous solution (25°C, I=0.1 M) from ref. 38; [f] ref. 39; [g] ref. 40; [h] pM at pH 7.4 in water (ref. 41 and 42).

Table 3 – ESI-MS ions for the Fe(III) and Cu(II) complexes of **6** and **16** in aqueous solution (1:1 and 1:2 Cu/L, $C_L = 6 \times 10^{-4}$ M; 1:3 Fe/L, $C_L = 1.2 \times 10^{-3}$ M).

Species	M=Fe (m/z) L=**6**	M=Cu (m/z) L=**6**	M=Cu (m/z) L=**16**
$[M(HL)Cl]^+$	-	386.2/388.2	-
$[M_2L_3]^+$	-	983.9/985.9	-
$[ML_2H]^+$	-	-	999.8/1001.9
$[M(HL)_2Cl]^+$	-	-	1035.5/1037.5
$[M(HL)Cl_2]^+$	413.5/415.5	-	-
$[ML(HL)_2Cl]^+$	952.8/954.8	-	-
$[ML_3Cl]^-$	950.5/952.5	-	-

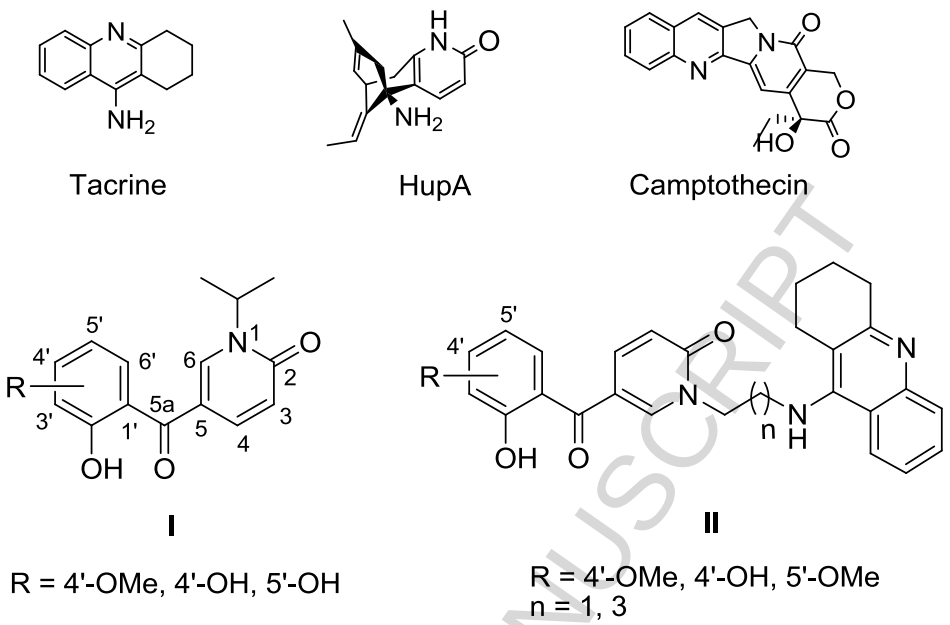

Fig. 1 - Molecular structure of: anti-AD drugs - tacrine and huperzine A (HupA) –, antitumour camptothecin and HBP derivatives under study (**I**, **II**).

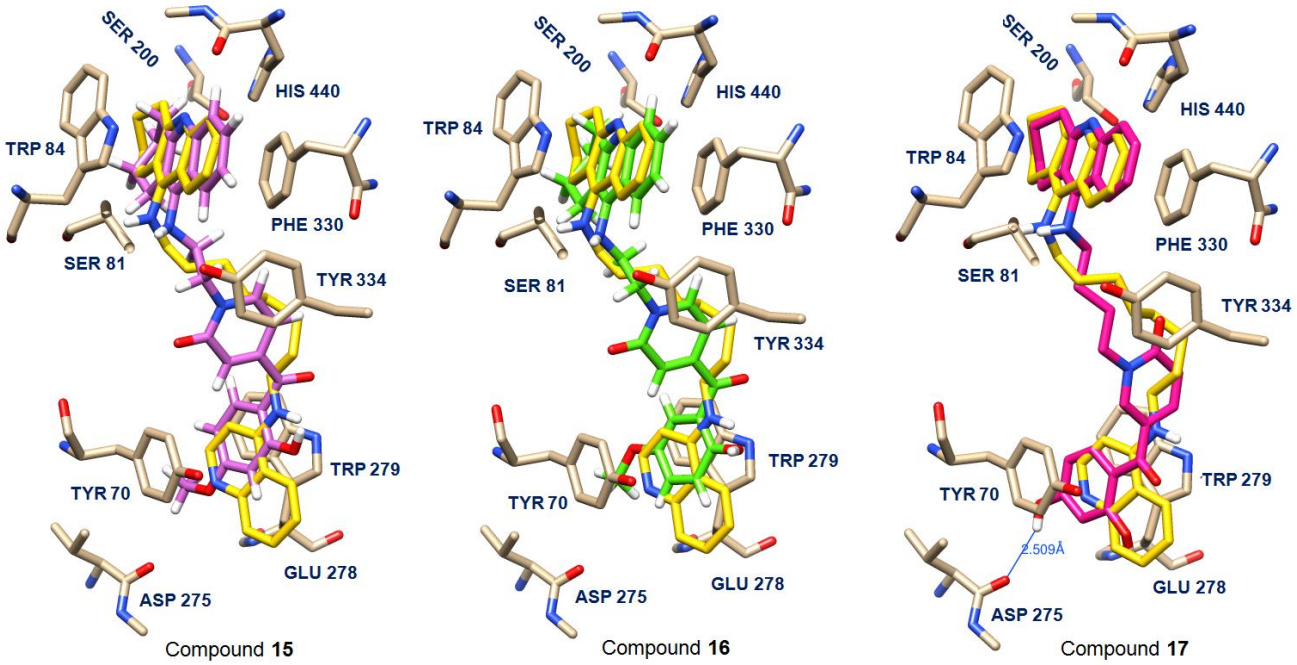

Fig. 2 - Docking of TAC-HBP hybrids into AChE: superimposition of **15** (violet), **16** (light green) and **17** (pink) with original ligand *N*-quinolin-4-yl-*N*'-(1,2,3,4-tetrahydroacridin-9-yl)octane-1,8-diamine (yellow). H-bond is represented as a solid sky-blue line.

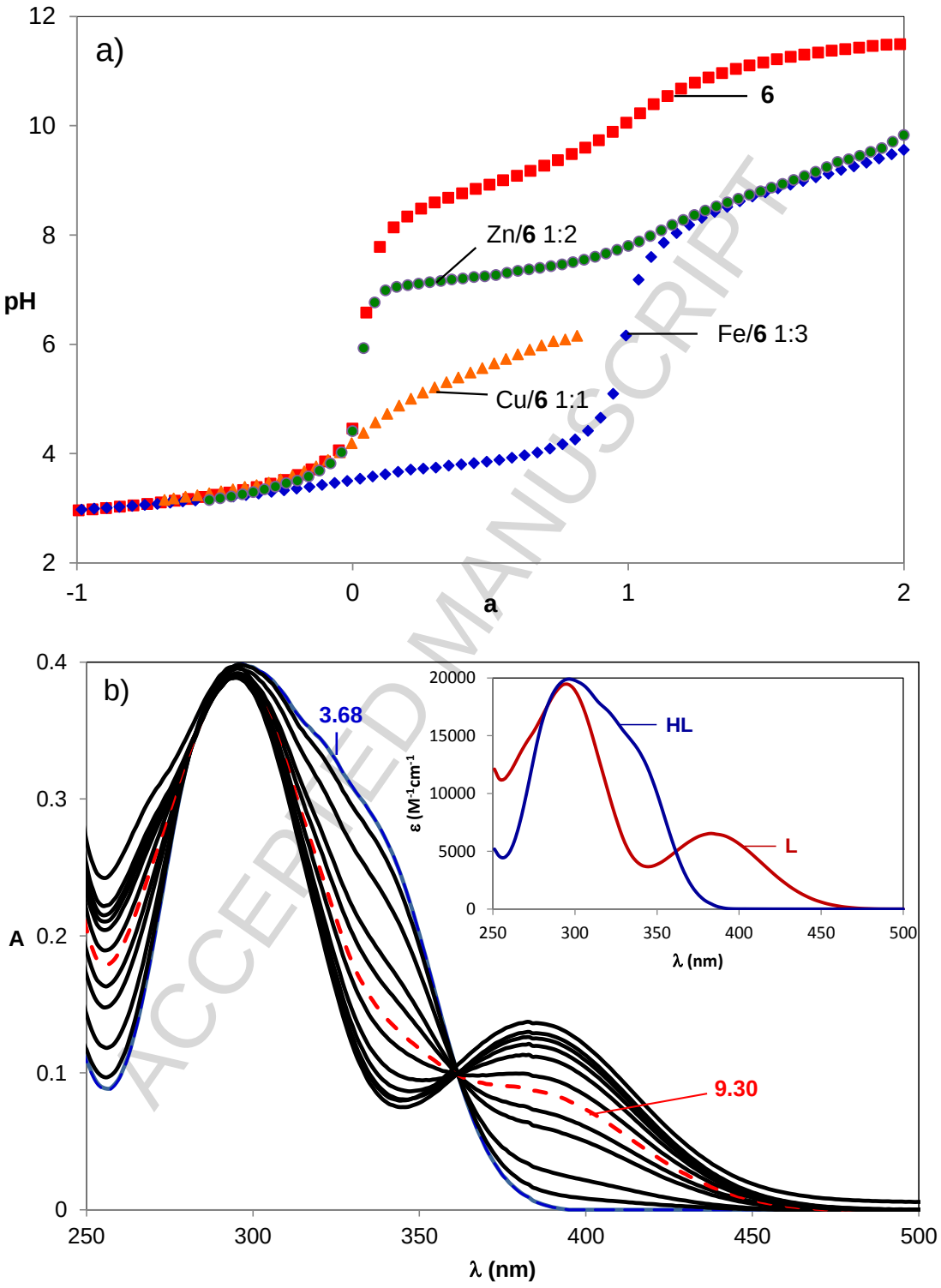

Fig. 3 - a) pH-potentiometric titration curves of **6** (C_L = 1 × 10^{-3} M); b) Spectrophotometric absorption spectra of **6** recorded for 3.68 < pH < 11.05 (C_L = 2 × 10^{-5} M) and inset containing the individual calculated spectra by PSEQUAD.

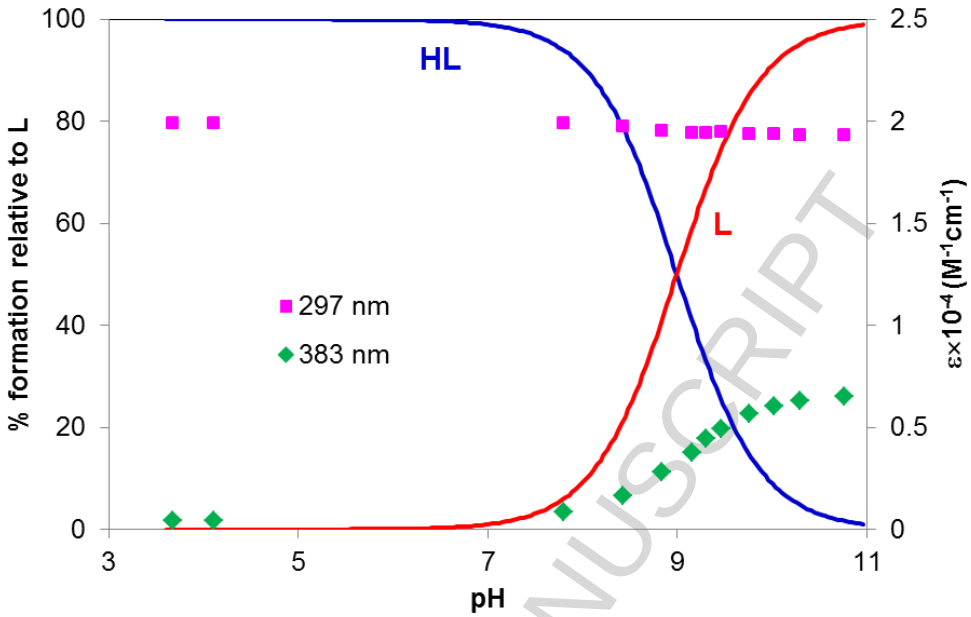

Fig. 4 - Species distribution curves for **6** with molar extinction coefficients at the maximum absorption wavelengths ($C_L = 2 \times 10^{-5}$ M).

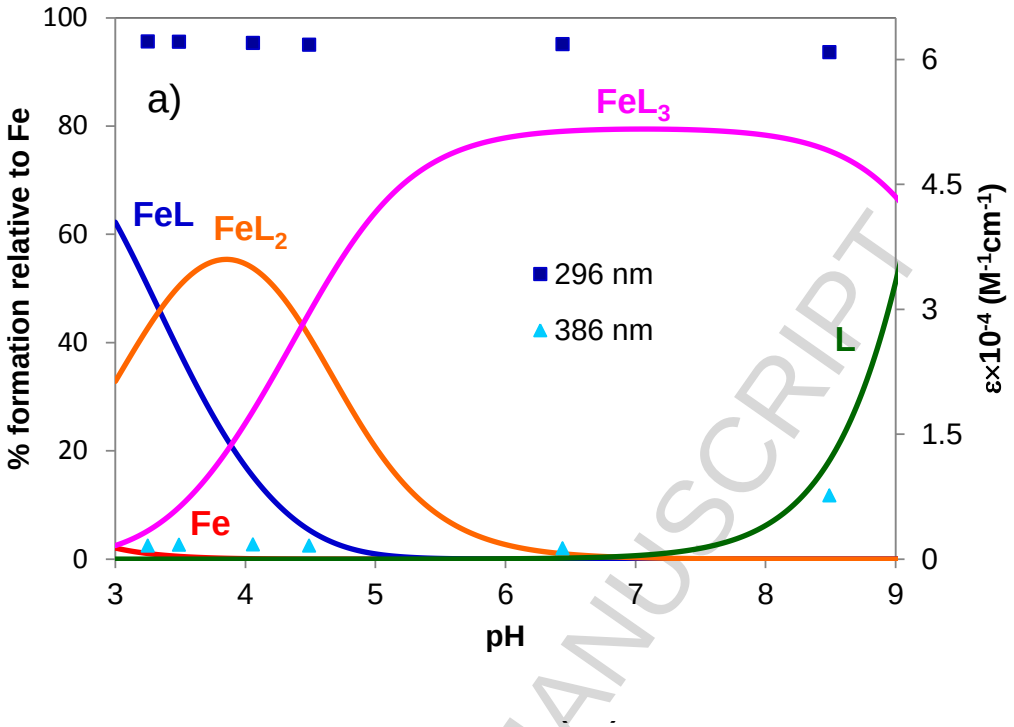

Fig. 5 – a) Species distribution curves for the 1:3 Fe(III)/**6** system with molar extinction coefficients at the maximum absorption wavelengths (C_L = 3.75 × 10^{-5} M); b) Spectrophotometric absorption spectra of **6** (pH = 7.80, C_L = 2 × 10^{-5} M) and Fe(III)/**6** 1:3 (pH = 6.44, C_L = 3.75 × 10^{-5} M).

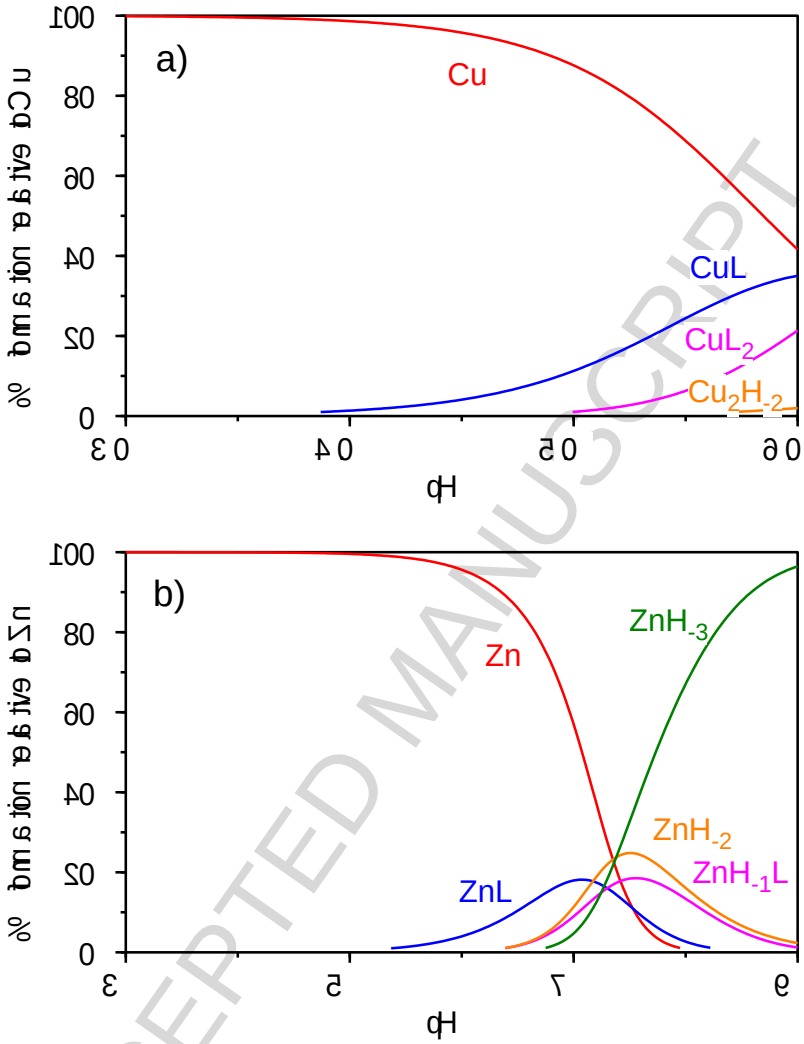

Fig. 6 - a) Species distribution curves for the 1:2 Cu(II)/**6** and b) 1:1 Zn(II)/**6** systems ($C_L = 1 \times 10^{-3}$ M).

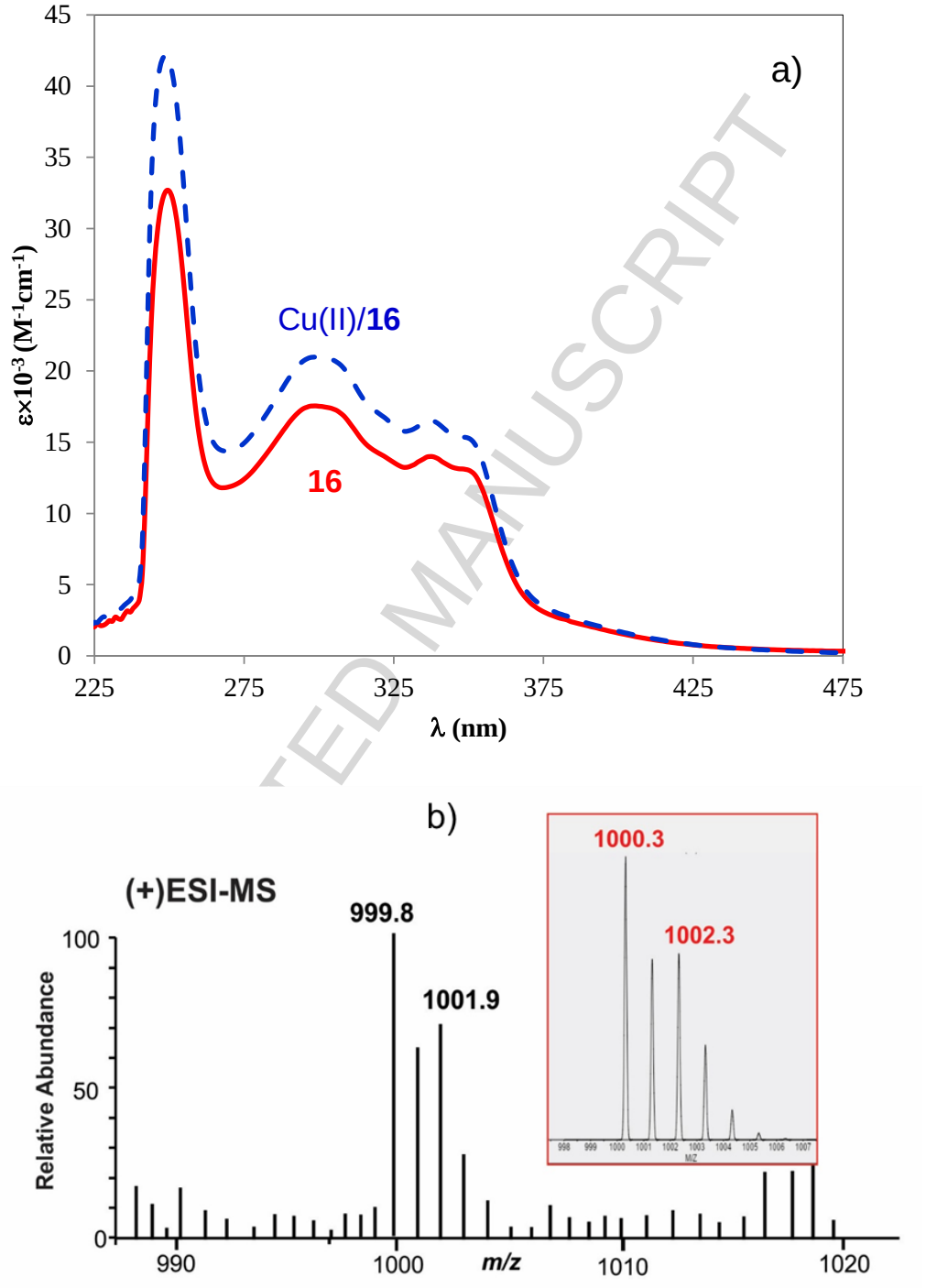

Fig. 7 – a) Spectrophotometric absorption spectra of **16** and Cu(II)/**16** 1:2 (pH = 7.40, C_L = 2×10^{-5} M); b) Expanded ESI(+) mass spectrum of Cu(II)/**16** 1:1 (pH=6.0, C_L = 6×10^{-4} M) showing a group of peaks at *m/z* 999.8 /1001.9 attributed to $[CuL_2H]^+$ species. The inset presents the calculated isotopic pattern for the cation $[C_{56}H_{53}CuN_6O_8]^+$.

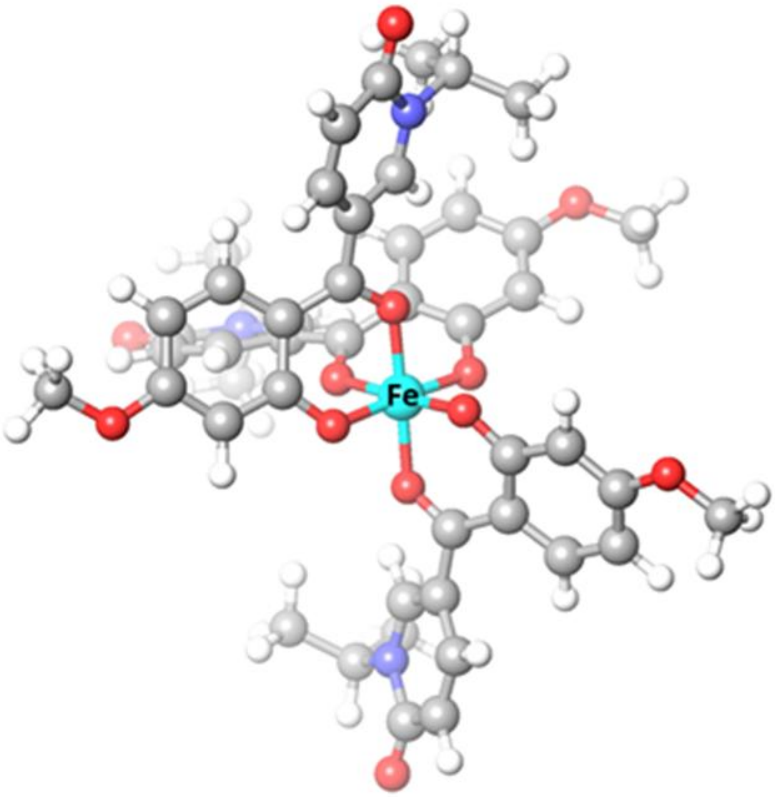

Fig. 8 - DFT-minimized structure of the FeL_3 complex of compound **6**. Coloring of atoms: Fe turquoise, N blue, O red, C grey and H white.

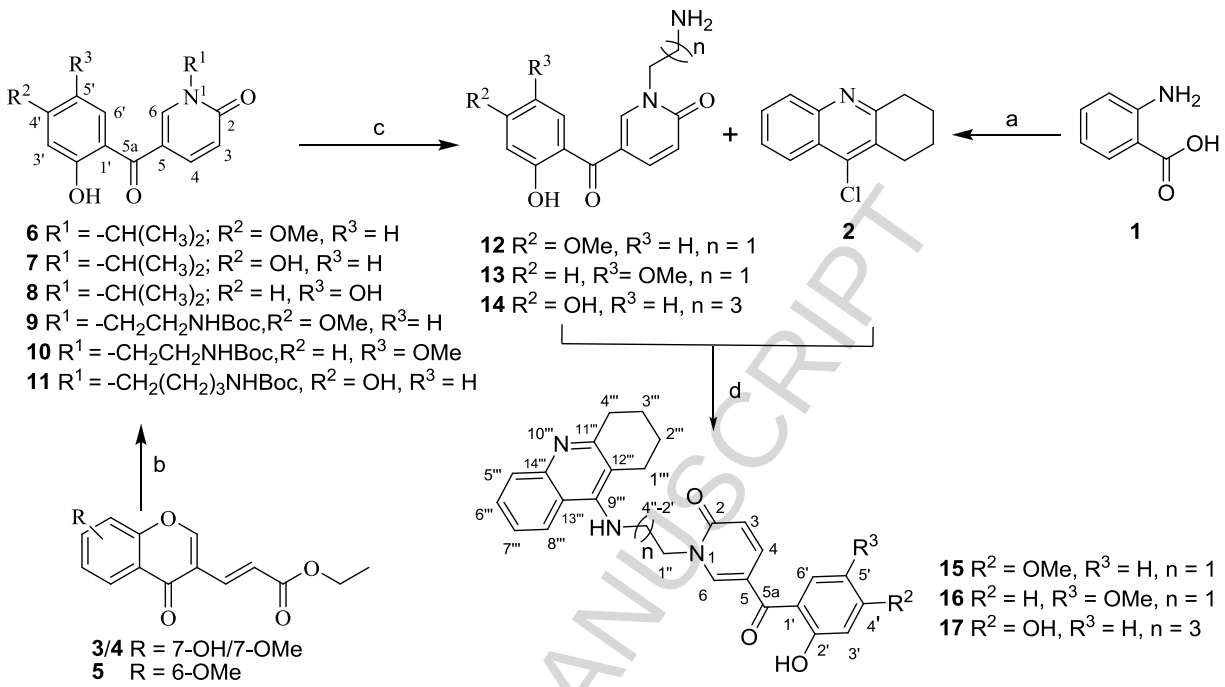

Scheme - Synthesis of HBP derivatives. Reagents and conditions: a) cyclohexanone, $POCl_3$, 180 ^oC, 4 hrs; b) R^1NH_2 (1.05 eq), NEt_3 (1-2 drops), C_2H_5OH, reflux, 8-10 h; c) DCM, TFA, 7-8 hrs; d) Phenol, KI, 165-170 ^oC 15 min.

Graphical abstract

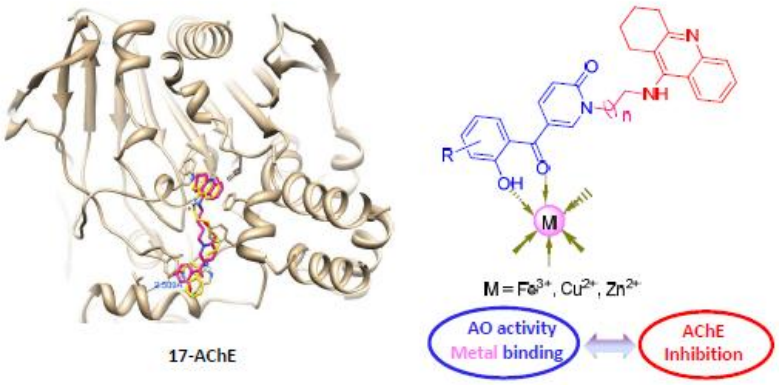

Tacrine-(hydroxybenzoyl-pyridone) hybrids were designed, synthesized and evaluated as potential multitarget anti-Alzheimer´s disease drugs. They are dual-binding site acetylcholinesterase inhibitors, with sub-micromolar activity as the parent tacrine, while the hydroxybenzoyl-pyridone moiety assures good radical scavenging capacity and moderate/good chelating power towards redox-active and/or amyloid-β-binding metal ions (Fe, Cu, Zn).

Highlights

- Tacrine-hydroxybenzoylpyridone hybrids (TAC-HBP) are designed and evaluated
- TAC-HBP are potential multitarget anti-Alzheimer´s disease agents
- TAC-HBP act as dual-binding site acetylcholinesterase inhibitors in submicromolar range
- The HBP moiety in conjugates is responsible for antioxidant & metal modulation
- TAC-HBP are moderate/good chelators of biometals (Fe, Cu, Zn)